Terrestrial 10 Be and electron spin resonance dating of fluvial terraces quantifies quaternary tectonic uplift gradients in the eastern Pyrenees

Magali Delmas, Marc Calvet, Yanni Gunnell, Pierre Voinchet, Camille Manel, Regis Braucher, Hélène Tissoux, Jean-Jacques Bahain, Christian Perrenoud, Thibaud Saos

Quaternary Science Reviews 193 (2018) 188–211

Contents lists available at ScienceDirect

Quaternary Science Reviews

journal homepage: www.elsevier.com/locate/quascirev

Terrestrial ^{10}Be and electron spin resonance dating of fluvial terraces quantifies quaternary tectonic uplift gradients in the eastern Pyrenees

Magali Delmas [a, *], Marc Calvet [a], Yanni Gunnell [b], Pierre Voinchet [c], Camille Manel [a], Régis Braucher [d], Hélène Tissoux [e], Jean-Jacques Bahain [c], Christian Perrenoud [c], Thibaud Saos [a], ASTER Team[d, 1]

[a] Université de Perpignan Via Domitia, UMR CNRS 7194 Histoire naturelle de l'Homme Préhistorique, 52 Avenue Paul Alduy, 66860, Perpignan, France
[b] Université de Lyon, CNRS UMR 5600 Environnement, Ville, Société, 5 Avenue Pierre Mendès-France, F-69676, Bron Cedex, France
[c] Museum National d'Histoire Naturelle de Paris, Institut de Paléonthologie Humaine, UMR CNRS 7194 Histoire naturelle de l'Homme Préhistorique, 1, Rue René Panhard, 75013, Paris, France
[d] Aix-Marseille Université, CNRS-IRD-Collège de France, UM 34 CEREGE, Technopôle de l'Environnement Arbois-Méditerranée, BP80, 13545, Aix-en-Provence, France
[e] BRGM, DGR/GAT, 3 Avenue Claude Guillemin, BP 36009, 45060, Orléans, France

ARTICLE INFO

Article history:
Received 22 February 2018
Received in revised form
28 May 2018
Accepted 1 June 2018
Available online 26 June 2018

Keywords:
Pleistocene
Alluvial terrace chronosequence
Electron spin resonance
Terrestrial cosmogenic nuclide
Fluvial incision
Topographic uplift
Neotectonics

ABSTRACT

The 120 km -longTêt River flows out of the Pyrenees to the Mediterranean. By displaying a mappable sequence of Quaternary alluvial units between the Pleistocene frontal moraines of the high range and the offshore sedimentary depocentres, its 1400 km^2 watershed is well suited to quantifying gradients of topographic uplift. Five main generations of terrace treads had previously been inferred from constrasts in regolith weathering features, but here we present the first radiometric age constraints based on 15 ESR sediment burial ages covering the full sequence, and 3 vertical TCN age profiles restricted to three mid-sequence terraces. Analytically robust results were obtained for the oldest and uppermost terrace T5 (ESR age: 1099 ± 179 ka), for T3b (ESR age: 374 ± 47 ka, ~MIS 10), and for T2 (ESR age: 174 ± 44 ka, ~MIS 6). These results are consistent with the contrasts in weathering grade of the deposits. The TCN profiles only yielded minimum exposure ages but provided precise post-depositional denudation rates for the fluvial terrace treads. The land-to-sea geometry of the chronosequence also provided clues about valley incision rates in response to topographic uplift during the last ~1 Ma. Based on a critical review of similar data obtained for other Mediterranean and Atlantic watersheds in the Pyrenees, the full regional correlation reveals that post-orogenic topographic uplift was substantial and relatively uniform throughout the entire mountain range. Patterns and magnitudes suggest a shared, probably subcrustal driving mechanism of Neogene and Quaternary mountain growth, with only subsidiary influence from isostasy, and climatic forcing.

1. Introduction

A fluvial terrace is an abandoned floodplain currently separated from the modern floodplain, or from a lower fluvial terrace, by a steeper slope, or scarp. Valleys often contain flights of multiple terraces that record the response of the fluvial system to environmental change in the watershed (Merritts et al., 1994; Blum and Törnqvist, 2000; Gibbard and Lewin, 2009; Pan et al., 2003, 2009; Bridgland and Westaway, 2014; Counts et al., 2015; Bridgland et al., 2017; Gao et al., 2017; Silva et al., 2017). Fluvial systems evolve under forcing factors such as the topographic and lithological attributes of watersheds, climatic change (which affects the ratio of water and sediment inputs from the slope system, and thus stream/resisting power) and base-level changes — whether driven by tectonics or eustasy (Leopold et al., 1964; Schumm, 1969, 1977; 2007; Bull, 1991). Given the constant interplay of these external variables, fluvial systems have been described as being in a permanently transient state (Finnegan et al., 2014), but they nonetheless exhibit a certain capacity to self-regulate, and thereby

* Corresponding author. UMR CNRS 7194 Histoire naturelle de l'Homme Préhistorique, Université de Perpignan Via Domitia, 52 avenue Paul Alduy, 66860, Perpignan, France.
E-mail addresses: magali.delmas@univ-perp.fr (M. Delmas), calvet@univ-perp.fr (M. Calvet), yanni.gunnell@univ-lyon2.fr (Y. Gunnell), pvoinch@mnhn.fr (P. Voinchet), manel@gmail.com (C. Manel), braucher@cerege.fr (R. Braucher), h.tissoux@brgm.fr (H. Tissoux), bahain@mnhn.fr (J.-J. Bahain), perrenoud@mnhn.fr (C. Perrenoud), thibaud.saos@univ-perp.fr (T. Saos).
[1] ASTER TEAM: Georges Aumaître, D. Bourlès, K. Keddadouche.

https://doi.org/10.1016/j.quascirev.2018.06.001
0277-3791/

maintain a relatively steady state at certain time and length scales (Schumm, 1973, 1979; Schumm and Parker, 1973). On that basis, each fluvial terrace in a sequence is commonly considered to be the legacy of a river longitudinal profile previously in dynamic equilibrium (Pazzaglia, 2013). Based on this criterion, incision rates deduced from terrace staircases are commonly used as proxies for quantifying crustal uplift rates (Maddy, 1997; Maddy et al., 2000; Maddy and Bridgland, 2000; Antoine et al., 2000; Brocard et al., 2003; Starkel, 2003; Westaway et al., 2006, 2009; Carcaillet et al., 2009; Pan et al., 2009; Viveen et al., 2012; Fuchs et al., 2013, 2014; Gallen et al., 2015; Wang et al., 2015; Ruszkiczay-Rüdiger et al., 2016; Olszak, 2017). The longitudinal profiles of bedrock rivers are also excellent indicators of active tectonics (Whipple, 2004; Whipple et al., 2013; Wobus et al., 2006; Demoulin et al., 2017).

Here we focus on the Pyrenees, a mountain range estimated from GPS data to be tectonically quiescent in most of its segments (Rigo et al., 2015), but where kilometre-scale topographic uplift during the last 10 Ma has been inferred from geological and geochronological criteria (Calvet and Gunnell, 2008; Gunnell et al., 2008, 2009). Quaternary fluvial incision inferred from alluvial terrace radiometric ages has only been documented so far within the northern and southern piedmonts belts (see Fig. 1, references therein and Stange et al., 2012, 2016). This paper presents the first radiometric ages obtained for a sequence of alluvial terraces in the eastermost part of the Pyrenees, where the 120 km-long Têt river connects the 2.8 km-high Carlit massif to the Mediterranean Sea and displays an exceptionally continuous Pleistocene fluvial sequence from the continental shelf almost all the way to the Würmian terminal moraines of the catchment headwaters. The approach is based on a conjugation of two independent methods: terrestrial cosmogenic ^{10}Be ages obtained from vertical depth profiles in the fluvial terrace deposits, and ESR ages of optically bleached quartz grains from the alluvial units. Age constraints on the five generations of fluvial terraces of the Têt watershed offer a unique opportunity (i) to quantify Pleistocene fluvial incision patterns along a continuum from the elevated headwaters to the coastal plain, and (ii) to discuss the driving mechanisms of Pleistocene surface uplift and crustal deformation in the Eastern Pyrenees. These results from the Têt are subsequently embedded in a critical review of the ages of previously dated fluvial sequences throughout the entire Pyrenean range, thereby providing an updated regional synthesis on the behaviour of Pyrenean rivers flowing to the Atlantic and Mediterranean base levels in response to Quaternary climatic change and tectonic forcing.

2. Geological and geomorphological setting

2.1. The Pyrenees: early cenozoic collision followed by neogene extension

The Têt watershed is almost entirely confined to the Axial Zone of the Pyrenees, i.e. the most elevated spine of the orogen (Fig. 1b). The Pyrenees formed as a result of collision between Europe and the Iberian microplate during and after the late Cretaceous. Collision-related deformation in the central and western Pyrenees ceased ca. 20–25 Ma, and by 30–28 Ma the eastern Pyrenees underwent NW–SE crustal extension, initially related to the opening of the Western Mediterranean back-arc basin (Durand et al., 1999). During the Neogene, extensional tectonics continued and formed a population of half-grabens all currently connected to one another by the Têt valley. From source to sea, these are successively the Capcir, Cerdagne, Conflent, and Roussillon basins. The first two contain an Upper Miocene continental sedimentary sequence (12–6 Ma), which is well preserved and dated in the Cerdagne and partially preserved in the Conflent (see Calvet, 1996; Calvet and Gunnell, 2008 for a synthesis). The last two contain a well-dated Lower to Middle Miocene continental aggradational sequence (24–15 Ma) covered by a prograding Pliocene sequence (5.3–3 Ma). A post-Miocene compressional to transpressional tectonic regime caused reverse- and shear-faulting on the boundary faults of the basins. The deformation has locally affected the Quaternary deposits (Phillip et al., 1992; Calvet, 1996, 1999; Goula et al., 1999; Lacan and Ortuño, 2012).

2.2. Neogene landscape evolution of the Pyrenees

At the end of the Oligocene and during the middle Miocene, two well-dated erosion surfaces bevelled parts of the Pyrenean structures, with remnants best preserved in the eastern (Birot, 1937; Calvet, 1996; Calvet and Gunnell, 2008; Gunnell et al., 2008, 2009) and central (Ortuño et al., 2008, 2013) parts of the range. The older erosion surface forms low-relief topography on massif summits. The younger population of Miocene pediments has developed on the flanks of some massifs, with a maximum relief of a few hundred metres of residual topography between the two generations of land surface. Two competing models exist for explaining the origin of these surfaces, with consequences for interpreting the chronology and drivers of valley incision and the resulting sequences of fluvial terraces in valleys such as the Têt. According to Bosch et al. (2016), the erosion surfaces were formed by altiplanation roughly at their current elevations as a consequence of raised base levels in the foreland basins (postulated as overfilled by sediment for the purpose of that scenario). This implies that mountain uplift peaked at the end of the Paleogene, and was followed by ca. 20 Ma of fluvial infirmity before the onset of valley incision, which would have been driven by major climatic changes at the end of the Neogene and by a component of isostatic rebound in response to the valley incision itself. The alternative model, tested in this study, is that the erosion surfaces formed at altitudes substantially closer to marine base level than at present. Regional subcrustal instabilities promoted uplift of these erosion surfaces in several successive stages during the last ~12 Ma. Valley incision was thus driven by post-orogenic regional uplift of the mountain range (Calvet, 1996, 1999; Calvet and Gunnell, 2008; Gunnell et al., 2008, 2009; Ortuño et al., 2008, 2013), as more recently confirmed by ^{26}Al/^{10}Be sediment burial ages at ~5 Ma and 1–2 Ma in alluvium-filled cave levels which are located at +270 m and +110 m, respectively, above the modern river channel in one short segment of the Têt valley (Calvet et al., 2015a; Sartégou et al., 2018). In order to test this hypothesis further, in this study we focus more widely on the Pleistocene incision chronology of the Têt River along its entire length and based on independent dating methods.

2.3. The Têt watershed

The shape and internal structure of the Têt watershed are strongly controlled by the Neogene basins and the major NE–SW-striking Têt–Cerdagne Fault (Fig. 1b). Above the town of Mont-Louis, the watershed headwater area strikes NW–SE and has incised a ~300 m-deep valley into the Carlit pediment. Around Mont-Louis, the Têt flows across the Plateau de la Perche (Figs. 2, 4a and 5), a younger rock pediment where the Paleozoic basement and the tectonically deformed Cerdagne Basin fill sequence are both bevelled by the low-gradient Perche topographic surface (Calvet, 1996; Calvet and Gunnell, 2008). Micromammalian fossils (bones, teeth) collected from the bevelled upper beds of the sedimentary fill sequence are Upper Miocene (~6 Ma; Agusti and Roca, 1987), and thus provide a maximum age for the Perche pediment. The pediment is the ancestral surface into which the Têt River began to

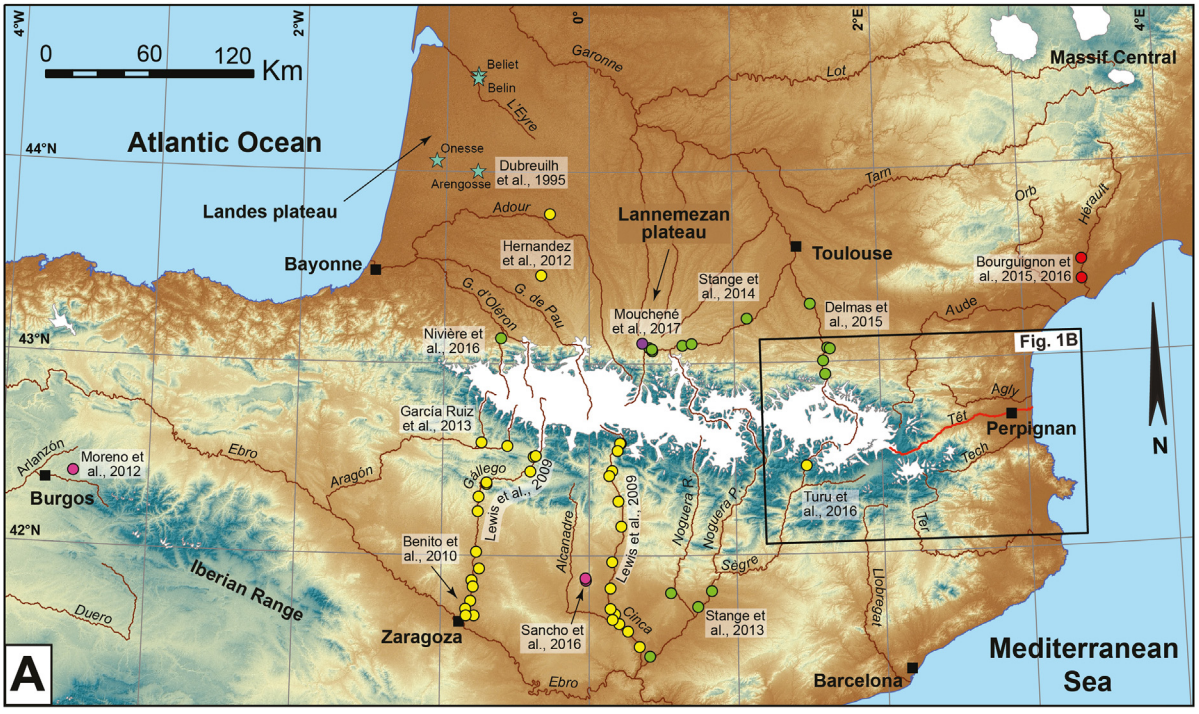

● ESR ● OSL ● TCN profiles ● TCN exposure ● $^{39}Ar/^{40}Ar$ ★ Biostratigraphic ages previously published

Late Pleistocene ice extent after Calvet et al., 2011. River network after HYDROSHEDS (Lehner & Grill, 2013).

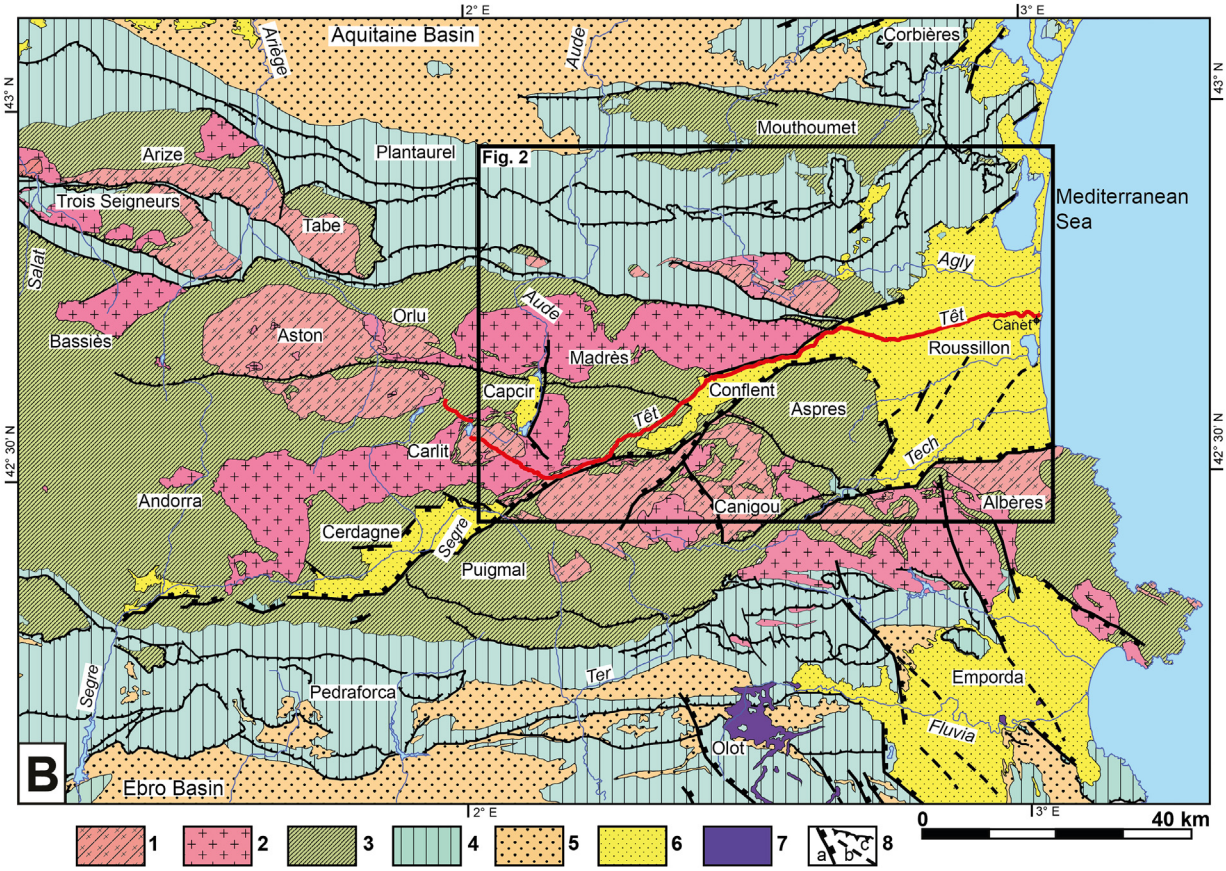

cut its deep valley after 6 Ma. The valley begins with a major knickzone >500 m high, just downstream of Mont-Louis (Fig. 5). After Mont-Louis, the Têt follows a SW–NE direction tightly aligned on the Neogene Cerdagne–Têt Fault and its wide crush zones, often flowing directly at the base of the escarpment's triangular faceted spurs. The valley flanks display a number of bedrock straths that grade topographically to the Plateau de la Perche. Many of these benches occur at elevations of ~. 1400 m along the southern flank of the valley, i.e. on the fault scarp itself (Fig. 4b). At the village of Thuès, the Têt drifts across the Conflent basin floor, then remains confined to the north side of the Conflent and Roussillon basins (bounded by the northern branch of the Têt Fault). The valley is epigenetic at several locations, i.e. it has cut into the underlying Paleozoic basement through the overlying clastic fill.

Downstream of Vinça, the Têt and its staircase of fluvial terraces become confined to benches cut into the Pliocene fill sequence of the Roussillon Basin. The Pliocene sequence has been interpreted as a Gilbert delta, which found the appropriate accommodation space at the time when the canyon subsequent to the brief Messinian Salinity Crisis became a drowned valley and rapidly filled with deltaic units that have been mapped in the lower Têt valley as far inland as Vinça (Clauzon and Cravatte, 1985; Clauzon et al., 1987, 1990; Clauzon, 1990; Duvail et al., 2005; Gorini et al., 2005). Most marine and continental outcrops in the Roussillon Basin are Zanclean. Aggrading and prograding wedges of Piacenzian and Gelasian age only occur offshore, with their delta fronts respectively situated 30 and 40 km from the present coastline. Onshore, the top of the continental topset beds has been dated to 3.8 Ma on the basis of micromammalian assemblages (Aguilar et al., 2007). However, four sites from surface karst cavities filled with abundant fluvial sand and gravel deposits containing rodent teeth, bone assemblages, and freshwater fish teeth indicate that fluvial sedimentation in the Roussillon Basin continued until ca. 2 Ma (Aguilar et al., 2007; Bachelet et al., 1990). Those palaeontological sites at Lo Fournas 13 and 16B (~3 Ma), at Pla de la Ville (~2.3 Ma), and Lo Fournas 4 (~2 Ma), are situated on the northern edge of the Roussillon Basin (Figs. 4g, 6 and 8). They occur on an erosion surface which functioned as the Têt River floodplain during Pliocene time and therefore provide — just like the Plateau de la Perche in the upper catchment — a 'terminus post quem', i.e. a topographic datum below which the Têt River began to cut a staircase of Pleistocene terraces into the Roussillon Basin. Given these independent biochronological contraints on the age of Lo Fournas plateau, the ages of the Têt terraces are expected to be younger than 2 ± 0.25 Ma (the analytical resolution of micromammalian biozones for the Pliocene is ~0.25 Ma: Aguilar and Michaux, 1987).

3. The Pleistocene fluvial sequence of the Têt

The Pleistocene sequence distinguishes itself from the underlying Pliocene sequence by the fact that it consists of thin alluvial sheets — 5–10 m maximum for each unit, and often much less in the case of the older and deeply weathered alluvial formations. These Quaternary deposits correspond to ribbons of braided gravel systems, up to 4–5 km wide, with a high potential for avulsion and perhaps not fundamentally different from the modern active channel systems. The disconformable boundary between the Pleistocene units and the underlying Pliocene sequences can be observed at the base of many vertical exposures (Fig. 9d and e).

3.1. A relative chronology based on multiple criteria

The criteria used until now for establishing the relative chronology of the terrace levels have been the post-depositional weathering intensity of the alluvial clasts and the characteristics of soils capping the terrace treads (Collina-Girard, 1975, 1976; Giret, 1995, 2014; Calvet, 1996; Debals, 1998, 2000). This method allowed 5 contrasting degrees of weathering to be distinguished above the present-day and earlier Holocene floodplains. On that basis, the Pleistocene fluvial sequence of the Têt was labelled T0 (modern plain) to T5 (uppermost terrace), and was correlated with the levels noted Fz (T0) to Fu (T5, sometimes also Fu-p) on the 1:50,000 scale geological maps of the region (Berger et al., 1988; Guitard et al., 1992; Fonteilles et al., 1993; Autran et al., 2005; Wiazemski et al., 2010; Calvet et al., 2015b). The most effective approach for characterising the post-depositional weathering intensity of the alluvial deposits was a semi-quantitative ranking procedure based on a 4-degree weathering-grade scale applied to different classes of clast lithology. The proportion of clay-sized particles in the sediment matrix and in Bt soil horizons, intensity of matrix rubefaction (Munsell redness index), and surface enrichment in residual quartz pebbles by relative accumulation, were also measured (Calvet, 1986, 1996; see Suppl. Information 1 for details).

Overall, the weathering and soil criteria provided diagnostic tools suited to defining generational bundles of fluvial terraces, but failed to discriminate between all of the topographically mappable terrace treads of the Têt sequence. For example, level T3 north of Perpignan consists of four distinct terrace treads labelled T3a to T3d from the lowest to the highest, each corresponding to alluvium-covered straths cut in the Pliocene substratum. The latter is exposed at the Llabanère and Courragade sections, with the Pliocene/Quaternary stratigraphic boundary occurring at a distinctly higher elevation at Courragade than at Llabanère (Figs. 2, 8 and 9d,e). Similar observations apply to T1.

3.2. Climatic control on terrace formation

The Têt watershed alluvial sequence results from a succession of climatically-driven aggradation–incision cycles. Two classes of evidence support this:

Firstly, all of the larger Pyrenean valleys present mappable evidence, usually underpinned by landform age constraints, of topographic connections between the treads of glaciofluvial terraces and Würmian frontal moraines. Such is the case for the Aude in the Capcir Basin (Fig. 2), for the Segre and its tributaries in the Cerdagne Basin (Calvet, 1996), for the Ariège (Delmas et al., 2011, 2015), the

Fig. 1. Location map. A. Numerical ages previously published on fluvial terrace systems in Pyrenees and surrounding areas. Note that along the strike of the central and western Pyrenees, outlet glaciers in the north (Ossau, Pau, Garonne, and Ariège watersheds) or to the inner fold and thrust belts in the south (Aragon, Gállego, Cinca, Nogueras watersheds) either destroyed or impeded the development of fluvial terraces within the most elevated core of the high range (known geologically as the Axial Zone). In the eastern Pyrenees, in contrast, Pleistocene glaciers were restricted to the upper valleys and allowed a more extensive development of fluvial terrace sequences (Segre, Têt, and Tech watersheds), which are still preserved deep in the Axial high range. B. Structural map of the eastern Pyrenees and study area. Key: Hercynian basement — 1: ortho- and paragneiss, migmatite. The large augengneiss bodies are Ordovician (475 and 445 Ma). 2: Hercynian (310–300 Ma) granitoids (granodiorite, leucogranite). 3: Ediacaran to Lower Paleozoic metasediments (micaschist, marble, chlorite schist, quartzite) and Caradocian to Lower Carboniferous sediments (schist, conglomerate, black shale, limestone, flysch). Mesozoic and Cenozoic cover — 4: Triassic to Eocene folded sedimentary cover (marl, limestone, sandstone, metamorphic marble and hornfels along the North Pyrenean Fault). 5: Eocene to Oligocene syntectonic continental conglomerates, molassic marl and sandstone of the foreland basins. 6: post-tectonic deposits (continental and marine) relating to the opening of the Western Mediterranean (Oligocene, Miocene, Pliocene). 7: Neogene basalt and trachyte (11–2 Ma) of Empordá; Quaternary volcanic rocks (0.4–0.02 Ma) of La Garrotxa. Tectonic features — 8a: Neogene normal faults; 8b: possible Neogene faults; 8c: synorogenic thrusts and reverse faults affecting the sedimentary cover and the basement. After Calvet (1996), simplified Lehner & Grill, 2013.

Cinca, Gállego, Aragon, Gave de Pau, Gave d'Aspe, Gave d'Ossau, Adour, and Garonne (Calvet et al., 2011; Cordier et al., 2017). In the case of the Têt, the topographic continuity between the Pleistocene moraines and the fluvial terraces has been erased along the 4 km bedrock knickzone downstream of the Mont-Louis (Fig. 5), but its previous existence can be reconstructed from the regional context (Fig. 2).

Secondly, farther downstream, a range of on- and offshore clues suggest that the Pleistocene terraces formed at the time of sea-level lowstands: (i) the geometry of reconstructed longitudinal profiles reveals that T1, T2 and T3 cross one another just downstream from Perpignan, then plunge beneath the Holocene and modern alluvial deposits (Fig. 6). The topographically elevated position of T5 all the way to the coastline (+10 m at Canet) suggests a tendency for the hinge line, or tilting point, to roll back westward over time, probably driven by subsidence of the continental shelf area in the east (Carozza and Delcaillau, 1999). (ii) Farther downstream from Perpignan, numerous borehole logs through the floodplain show, below the fine Holocene alluvium, very coarse cobble beds, which are attributed to the Pleistocene but of indistinguishable affinity with any specific generation of Pleistocene terrace farther upstream in the watershed (see open-access subsurface resources data bank, http://infoterre.brgm.fr/). (iii) Boreholes and seismic profiles along the coastline and foreshore near Leucate and Barcarès have revealed below the Holocene highstand system tract and Eemian highstand system tract incised and filled by a Würmian alluvial sequence. The entire sequence fills a palaeovalley striking SW–NE (Labaune et al., 2005; Duvail, 2008). (iv) On the inner continental shelf, two gravel beds connected to a palaeoshoreline −100 m below the present sea level (ca. 40 km from the modern coastline) yielded radiocarbon-dated cold-climate mollusc shells (ages ≥ 35 ka and 18.3 ± 0.75 ka BP) retrieved from the lower and upper units, respectively (Monaco et al., 1972; Monaco, 1973; Labeyrie et al., 1976). (v) Lastly, on the middle and outer continental shelf, very high resolution seismic reflection data associated with shallow cores revealed the existence of five regressional sequences (clinoform interpreted as a sets of littoral and offshore prodeltaic deposits), each cut by an erosional surface (as a result of subaerial and marine erosional processes acting respectively at times of falling and rising sea level). The regressional sequences have been correlated with the last five 100 ka cycles of the Middle and Late Pleistocene (Lobo et al., 2004; Rabineau et al., 1998, 2005, 2006, 2014). The uppermost sequence was radiocarbon-dated between 47 and 12 ka and characterised by pollen spectra (Beaudoin et al., 2005).

On land, the only two available ages derive from archaeological constraints and from radiocarbon ages obtained from Holocene levels in the Roussillon plain (Calvet et al., 2002; Carozza and Puig, 2011; Carozza et al., 2011, 2013) and from the lowermost Würmian terraces of the Verdouble and Réart watersheds (Fig. 1; Dubar, 1986; Giresse and Martzluff, 2015; Carozza et al., 2016). This paper presents the first effort to date the entire Pleistocene fluvial sequence of the Têt River. Terraces T1 to T5 were sampled at nine different

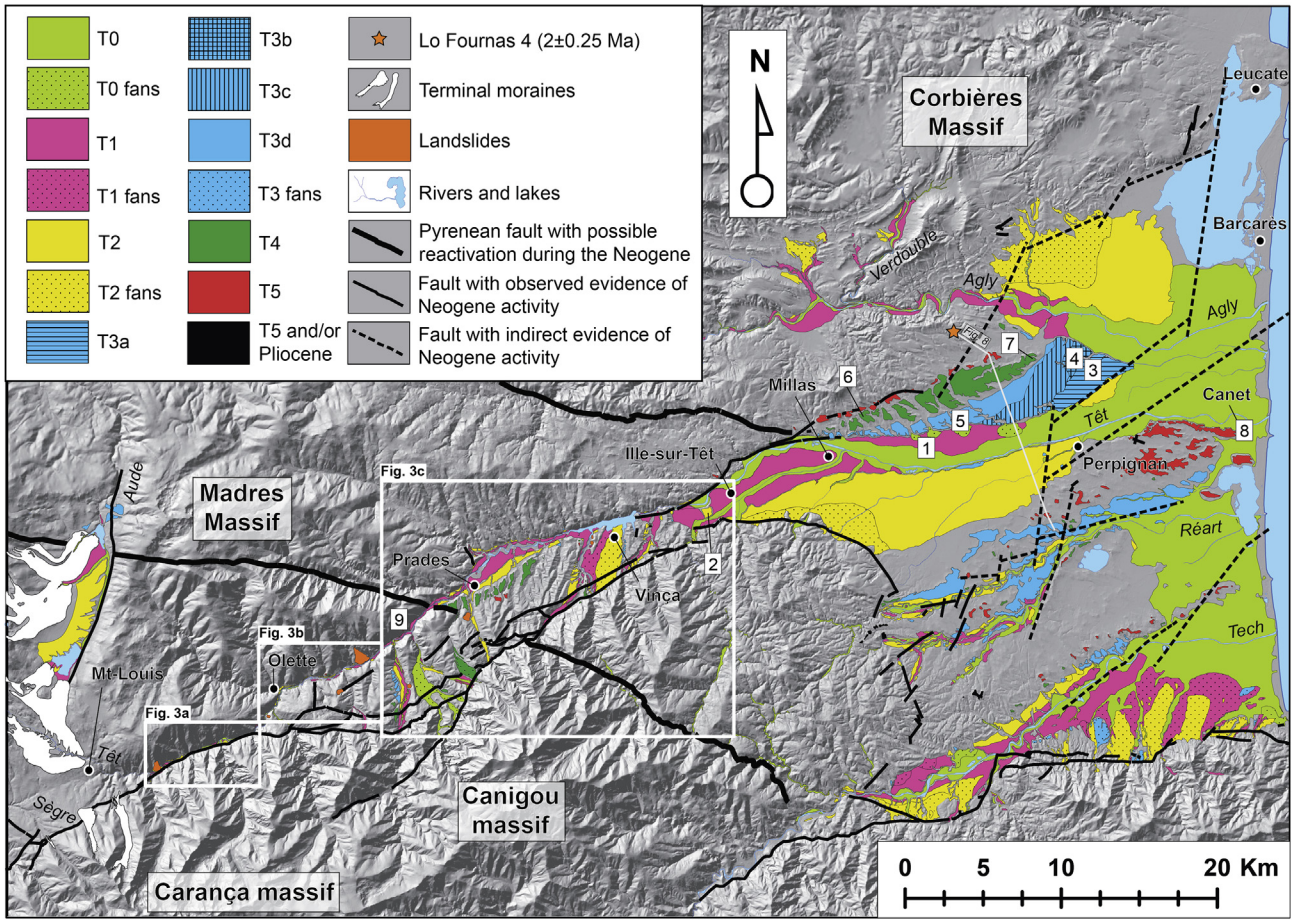

Fig. 2. Map of the Pleistocene fluvial terrace sequence of the Têt watershed. Sampling sites: 1. Pezilla, 2. Escatllars, 3. Llabanère, 4. Courragade, 5. Quatre Chemins, 6. Campeils, 7. Peyrestortes, 8. Canet, 9. Villefranche. Unornamented blue colour indicates undifferentiated T3 terrace levels in watersheds other than the Têt. (For interpretation of the references to colour in this figure legend, the reader is referred to the Web version of this article.)

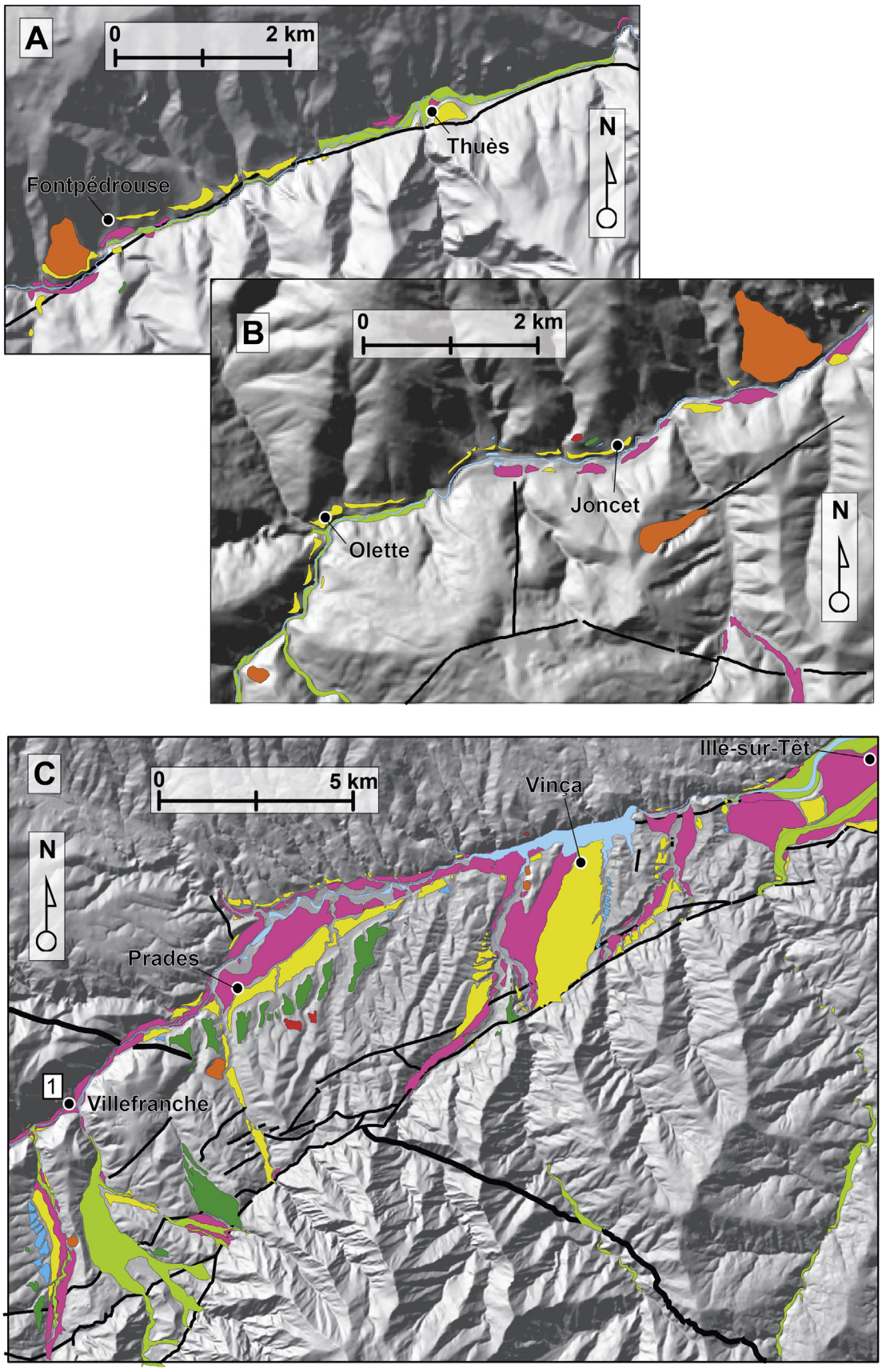

Fig. 3. Map of the Pleistocene fluvial sequence. Detail on the upstream area. See Fig. 2 for key to ornaments and symbols.

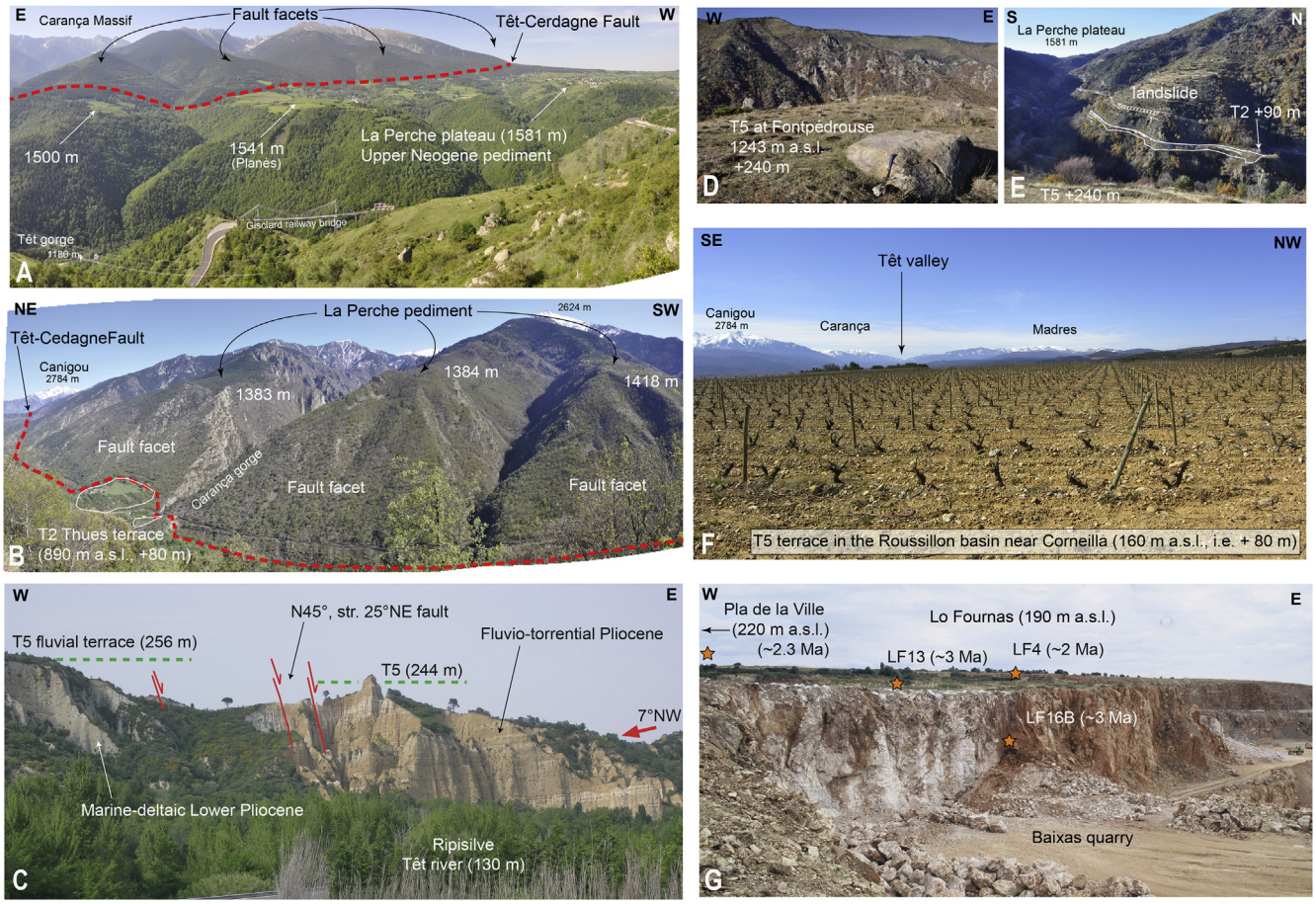

Fig. 4. Landscapes in the Têt watershed.

sites (Figs. 2, 6 and 7). Three of the sites benefited from paired terrestrial cosmogenic nuclide (TCN) and electron spin resonance (ESR) dating from identical levels for comparative purposes (Tables 1–3). The other six sites were dated exclusively using ESR because of unsuitable conditions for obtaining vertical TCN sampling profiles.

4. Methods

4.1. Fluvial terrace mapping and reconstruction of river palaeoprofiles

The six 1:50,000 scale geological sheets that encompass the Têt watershed area offer a fairly exhaustive coverage of all Pleistocene deposits (Berger et al., 1988; Guitard et al., 1992; Fonteilles et al., 1993; Autran et al., 2005; Wiazemski et al., 2010; Calvet et al., 2015b), but given the staggered publication of the maps over nearly 30 years, no coherent picture has spontaneously emerged from the basic map mosaic. A revision of polygon contours and an acquisition of geochronological constraints was necessary (Fig. 2). For this study, the entire collection of outcrop polygons was laid over the 1:25,000 scale maps of the Têt watershed (contour intervals: 10 m in upland areas, 2.5 m in the plains) in order to produce a much more precise geomorphological map of the fluvial terraces treads than previously afforded by the 1:50,000 scale geological maps. Terrace treads of a given generation were joined up from the terminal moraines near Mont-Louis to the continental shelf (Figs. 5–7), where the geometry of system tracts has been documented by geophysical surveys and interpolated borehole log data (Rabineau et al., 1998, 2005, 2006, 2014; Duvail and Le Strat, 2000; Duvail et al., 2001, 2002). The longitudinal profiles of each terrace unit in the landscape were plotted from hand-held global positioning system (GPS) coordinates and topographic-sheet spot heights (Figs. 5–7). All of the data points were projected orthogonally onto a longitudinal axis made up of segments each parallel to the local strike of the trunk stream. Correlation between upstream and downstream terrace-tread segments also took account of the elevations of tread levels relative to the altitude of the modern thalweg, and were backed up by the weathering criteria (Suppl. Information 1). Transverse valley sections also helped to constrain the spatial architecture of the terrace sequences and their substratum, with indications about deposit thicknesses obtained from the open-access BRGM subsurface resources data bank (Fig. 8).

4.2. TCN vertical profile dating

TCN accumulation in Earth-surface materials depends on the outcrop exposure history to cosmic rays and on the denudation that affects the investigated area. Theoretically, TCN concentrations decrease exponentially with depth as a result of the attenuation with depth of the particles involved in TCN production. The attenuation is directly proportional to material density. In the case of ^{10}Be, two main types of secondary particle with significantly different attenuation lengths, neutrons and muons are involved in nuclide production in rocks. Within 2 m below the topographic

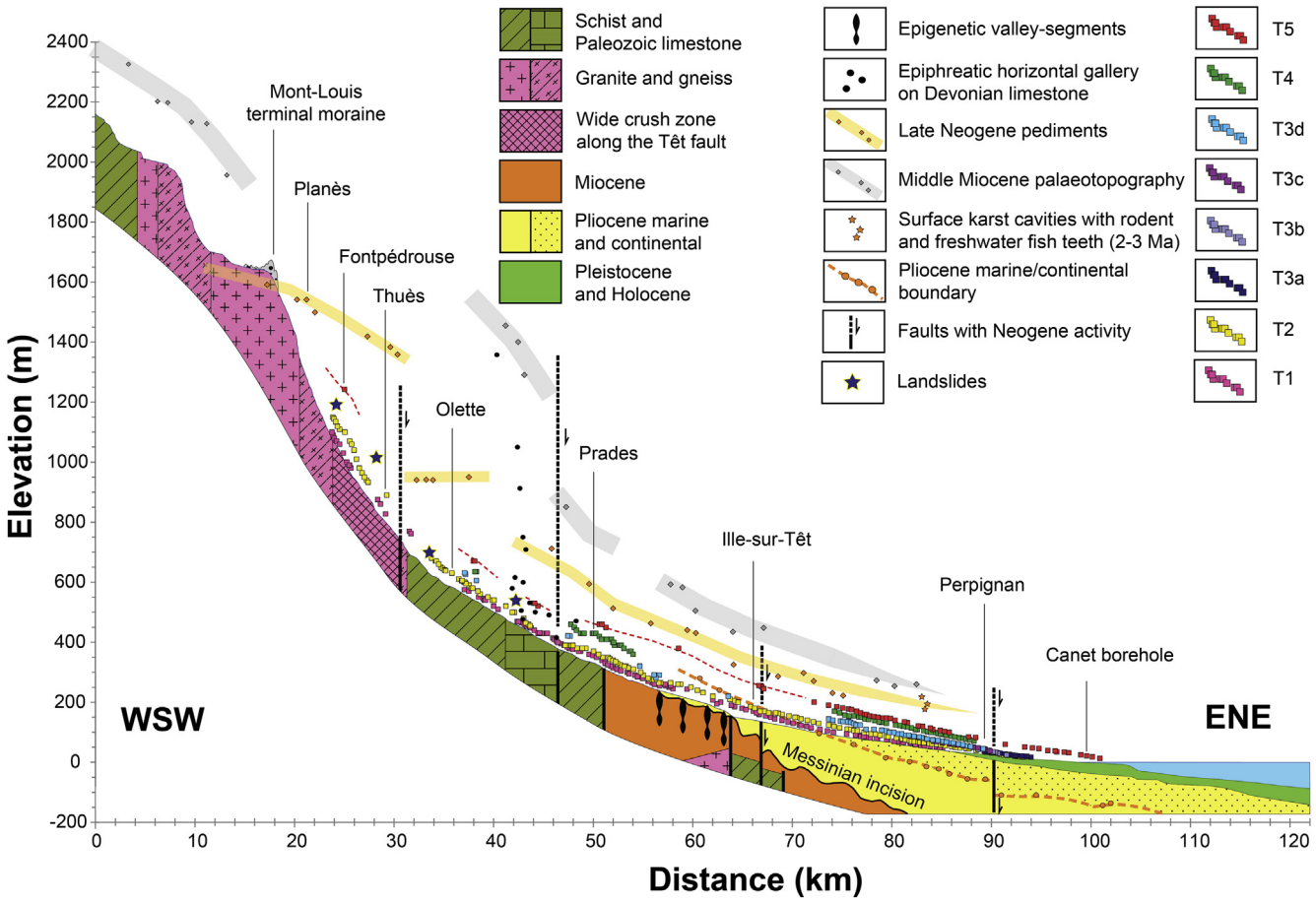

Fig. 5. Longitudinal profiles of the Têt terrace treads.

surface, neutronic production reaches a steady state (balance between nuclide production and nuclide decay for a given denudation rate) sooner than in the case of muonic contribution.

The vertical profile method consists in collecting several clast samples from the alluvial outcrop at carefully measured depths beneath the depositional surface (Table 1) and calculating a best fit between the ^{10}Be concentration in each sample and the theoretical depth–concentration curve that governs the accumulation of in situ-produced ^{10}Be atoms in the Earth's crust (Braucher et al., 2003, 2009, 2011, Rixhon et al., 2017). The quality of fit is estimated using the χ^2 statistical test. By this approach, it becomes possible to simultaneously calculate the best-fitting values for four different variables: (i) the exposure time of the abandoned floodplain surface (obtained from the muonic contribution that dominates the TCN production at depths greater than 2–3 m); (ii) the denudation rate responsible for potential terrace-tread lowering since the onset of fluvial incision (obtained from the neutronic contribution that dominates at depths shallower than 2–3 m); (iii) the mean density of all materials (from clay-sized to boulder-sized) exposed in the sampled profile over an angle of 2π steradian (the flux of cosmic rays to the Earth being isotropic); and (iv) the proportion of nuclide inheritance within the original clast population (owing to the fact that each transported particle feeding into the alluvial deposit arrives with a dose of ^{10}Be acquired during its pre-depositional history within the watershed. However, when TCN concentrations at the base of the profile (preferably below 2–3 m) have reached a steady state, data modelling allows a precise estimation of the post-depositional surface denudation rate but only provides a minimum exposure age for the terrace tread.

In order to take into account the different uncertainty levels around concentrations measured at different depths (Table 1), a Monte Carlo simulation is used to produce a multitude of best-fit solutions ($n = 100{,}000$ for each profile). The range of solutions thus produced is modelled from a range of concentration values randomly selected within the error band that affects all the measurements in the sampled profile, and all the obtained statistical solutions are theoretically possible. This routine is repeated iteratively for realistic sediment densities between 1.8 and 2.6, in accordance with the more commonly accepted values for clast-supported sediments (Vincent and Chadwick, 1994; Hancock et al., 1999; Hidy et al., 2010), for denudation rates between 0 and 2 cm·ka^{-1}, and for nuclide inheritance values between 0 and 10^6 at g^{-1}. According to Hidy et al. (2010), the most probable quadruplets of solutions are those that match the 100 smallest χ^2 value (Fig. 10, Table 2). In this study, we graded as acceptable any model with a χ^2 value situated between the smallest χ^2 value (termed: χ^2min) and [χ^2min+1] (Braucher et al., 2009) because this range of solutions is considered a mathematical substitute, or proxy, for the 1σ confidence interval (Bevington and Robinson, 2003).

The TCN vertical profile approach was applied to three exposures of terraces T2, T3c and T3d, respectively. The three vertical profiles analyzed were historically recent gravel-pit walls (Courragade on T3c) or highway embankments (Escatllars on T2, and Quatre Chemins on T3d). They are situated at a safe distance (> 5 m) from any naturally occurring stream incision, and sampled sections were suitably refreshed for the sampling procedure. Each profile totalled between 7 and 10 samples collected at the top of the terrace and along a vertical distance of 340–475 cm (Table 1). All

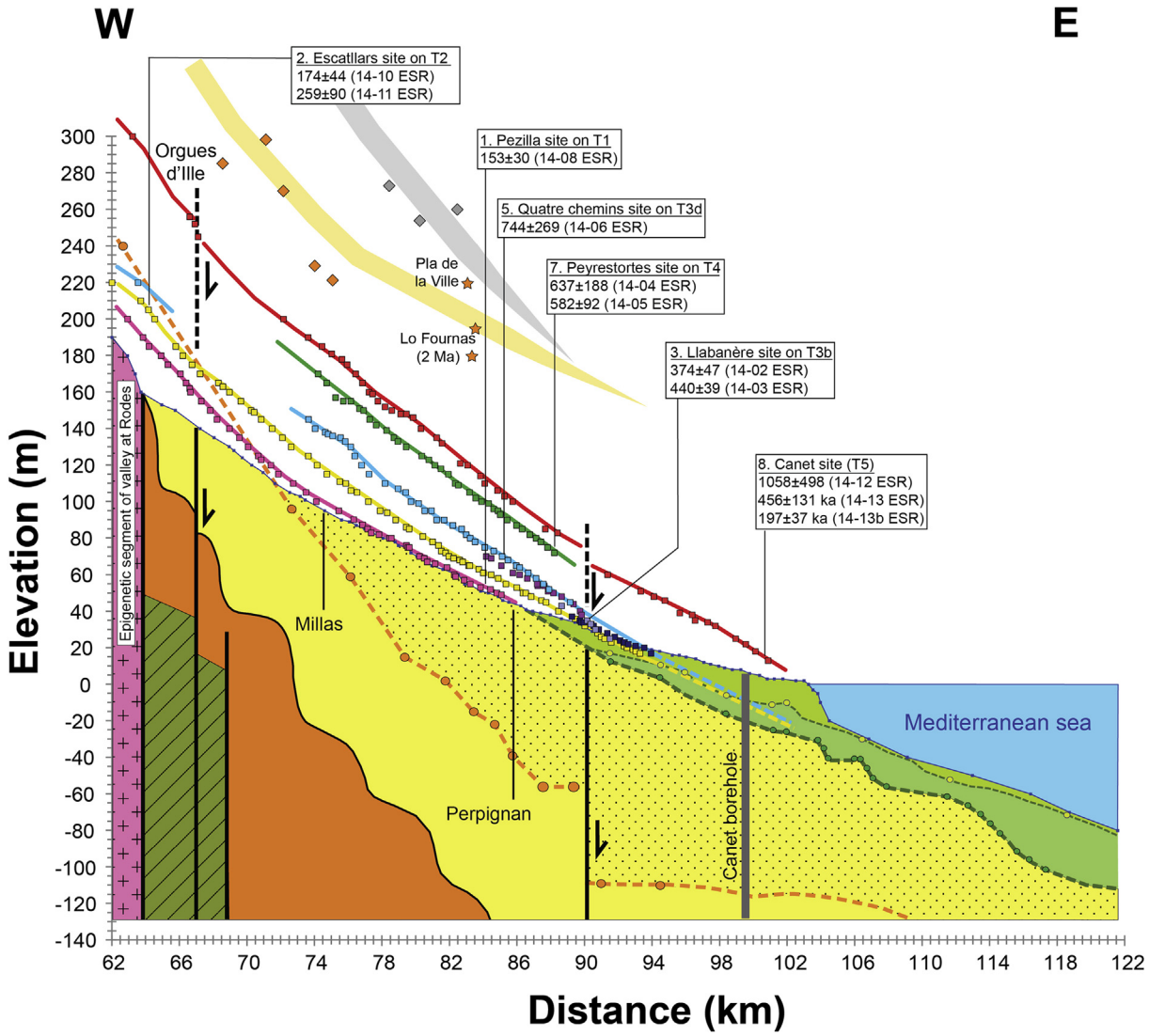

Fig. 6. Longitudinal profiles of the Têt terrace treads. Details of the downstream area. See Fig. 5 for key to ornaments and symbols.

the samples consisted of an aggregation of small quartz, granite and gneiss pebbles (long axis: 1–3 cm), occasionally including some sand from the surrounding matrix (see Suppl. Information 2 for details on the analytical procedure).

4.3. Electron spin resonance (ESR) dating

Electron spin resonance (ESR) dating is a palaeodosimetric method based on the study of light-sensitive signals generated by optically bleached natural crystals. The method here was based on the measurement in 100–200-μm-sized fluvial quartz grains of the accumulated natural radiation dose resulting from environmental radioactivity. ESR dating of quartz uses radiosensitive centres such as aluminium and titanium, which are both light-sensitive. Given that the corresponding ESR signals are reset by exposure to sunlight, it becomes possible to estimate the date of sediment deposition as the time when the last exposure to sunlight occurred before burial of the quartz grains. Depositional age is then derived by assessing the total dose of radiation received by the sample since its deposition (known as paleodose, or equivalent dose: *De*), divided by the annual dose rate (*Da*). The latter is obtained by measuring different radiation sources located in the sample itself and in its depositional environment (sum of alpha, beta, gamma and cosmic-ray contributions). Gamma dose rates were determined in the field using an Inspector 1000 gamma spectrometer. External alpha and beta contributions were calculated from the sediment radioelement contents (U, Th and K) as determined in the laboratory by high resolution and low background gamma-spectrometry. The total dose reconstruction was based on a Multiple Aliquot Additive (MAA) dose method, which is now the routine procedure for ESR dating of sedimentary quartz (see Suppl. Information 3 for fully referenced details on the analytical procedure). Analytical uncertainties are reported as $\pm 1\sigma$. The weighted average ages were calculated using IsoPlot 3.0 (Ludwig, 2003).

5. Results

5.1. TCN depth profiles

5.1.1. Escatllars profile (T2)

This profile is located on a 0.37 km^2 residual terrace strip 2 km downstream of the epigenetic gorge of Rodès, as the Têt River enters the Roussillon Basin (Figs. 2 and 6). The exposure in the embankment of a road slicing through the middle of the terrace

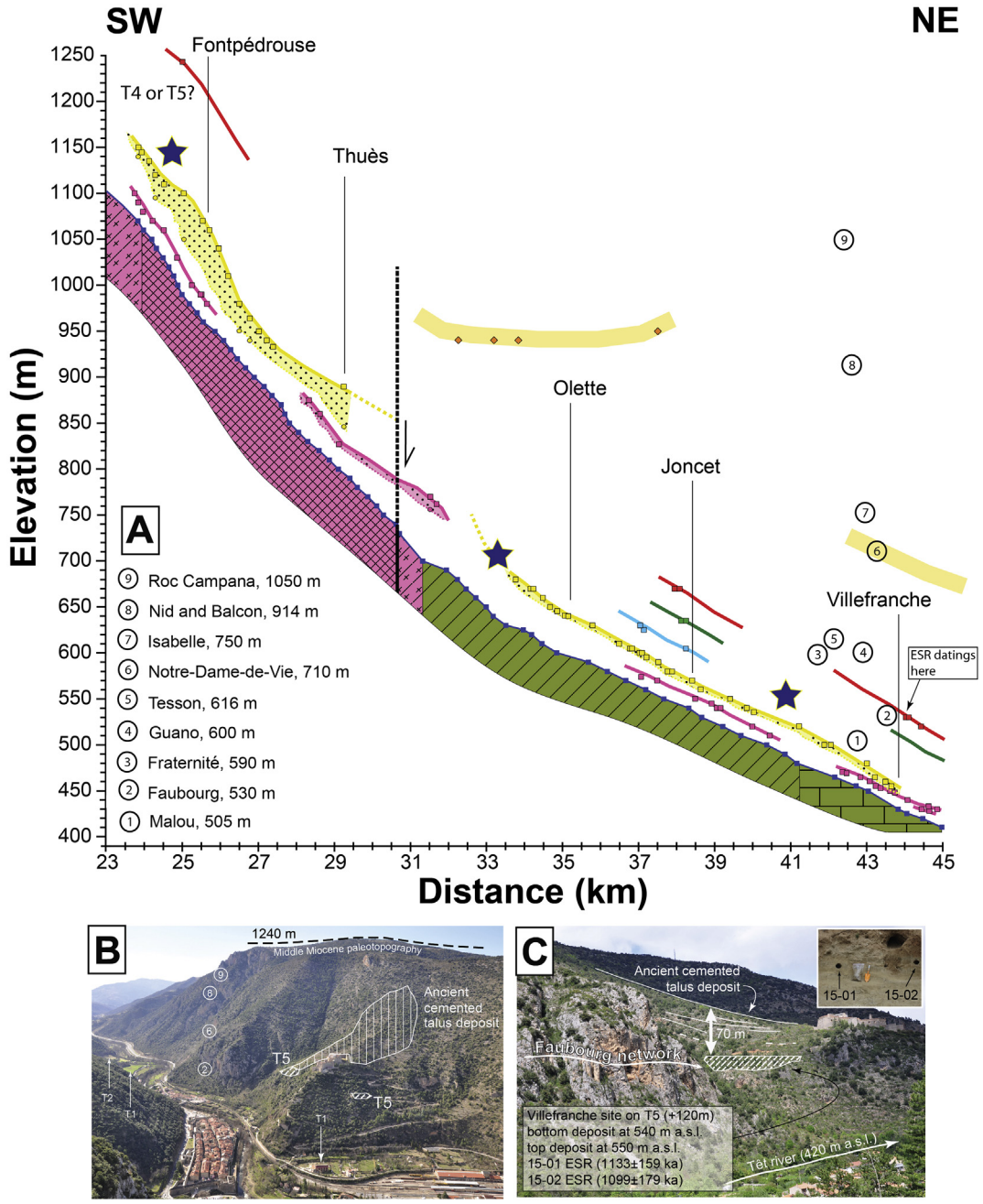

Fig. 7. Longitudinal profiles of the Têt terrace treads. A. Details of the upstream area (see Fig. 4 for key to ornaments and symbols). B, C. Relations between the Têt fluvial sequence and the phreatic cave level stack at Villefranche.

tread exposes 5–6 m of the alluvial formation (Fig. 9c). The section was refreshed prior to the collection of 7 samples over a depth of 4.75 m (Table 1). Only one sample yielded insufficient substance after chemical extraction to warrant ^{10}Be concentration measurements. TCN concentrations in the remaining 6 samples show a steady decline with depth and a very small misfit against the theoretical curve (Fig. 10). Modelling of the profile in the absence of predefined constraints on any of the four parameters of interest yielded only 32 acceptable model solutions falling within the [χ^2min; χ^2min+1] interval (blue dots in Fig. 10). This population of best fits covers a broad band of exposure ages from 369 to 976 ka, but a very narrow band of surface denudation rates (0.85–0.96 cm/ka). Note that the top 100 best-fit solutions yield a similar band of exposure ages and denudations rates (yellow dots in Fig. 10; see also Table 2). This indicates that all the TCN concentrations from this profile are close to attaining their maximum (i.e. steady-state) value. The minimum age among the 100,000 model solutions was 53 ka.

5.1.2. *Courragade profile (T3c)*

The Courragade profile is a vertical quarry face exposing T3c on the left bank of the Têt, on the northern edge of the Roussillon Basin (Figs. 2 and 6). Seven samples were obtained from the topsoil to a depth of 340 cm (Table 1, Fig. 9e–f). Each sample was a collection of small pebbles (long axis: 1–3 cm), almost exclusively of quartz except for the deepest sample, which also contained some sand

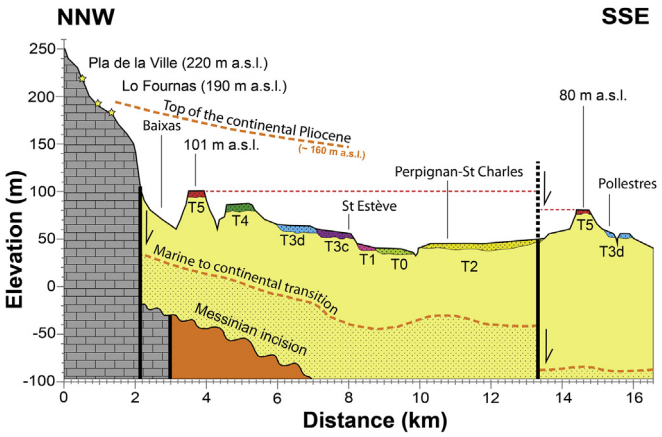

Fig. 8. Cross-profile of the Têt terrace sequence in the Roussillon Basin. Alluvial thicknesses and dips within the marine to continental Pliocene transition are inferred from the French national soil data bank (http://infoterre.brgm.fr/).

matrix. Three additional samples consisting of an amalgamation of 1–3 cm patinated quartz pebbles were collected from the soil surface on the terrace tread among vineyards immediately adjacent to the quarry in order to constrain TCN concentrations in the uppermost part of the alluvial deposit. Results show that TCN concentrations decrease quite steadily with sampling depth (Table 1, Fig. 10). In contrast, the surface samples display a wide scatter of nuclide concentrations. This is ascribable to the fact that the quartz clasts collected from the surface derive from a lag deposit generated by a lengthy period of in situ pebble weathering and matrix eluviation, resulting in the relative enrichment of the topsoil in residual quartz (the lithology least susceptible to weathering among the original mix) observed in terraces T5, T4 and T3. In T3, quartz clast concentrations of 82% occur in the topmost ~90 cm of the profile, whereas the initial alluvial mass contained just 23% of quartz. From this can be inferred a post-depositional loss of 2.3 m of alluvial thickness by chemical weathering and eluviation. As a result, a proportion of quartz debris collected at the surface today appears to contain a record of nuclide accumulation acquired at greater depths than meets the eye. Some of these clasts thus record a lower TCN concentration than clasts that have effectively resided at the surface of the terrace tread since the time of deposition.

While letting all four basic variables of interest behave unconstrained, model runs yielded 651 solutions falling in the [χ^2min; χ^2min+1] interval (blue dots in Fig. 10). This population of best fits covers an intractably broad band of exposure ages from 170 to 998 ka, but a narrow band of surface denudation rates (0–0.42 cm/ka). The denudation rates become even more precise (0.35–0.4 cm/ka) when the range of acceptable solutions is restricted to the 100 smallest χ^2 values (yellow dots in Fig. 10, Table 2). Such a distribution of age–denudation pairs indicates that TCN concentrations throughout the vertical profile satisfy the conditions of a nuclide steady state. The data modelling thus provides an excellent estimate of the post-depositional mean denudation of the terrace tread. The terrace 'age', in contrast, remains poorly constrained but is older than 170 ka based on the [χ^2min; χ^2min+1] best fit solutions. The minimum age among the 100,000 model solutions was 119 ka.

5.1.3. Quatre Chemins profile (T3d)

The Quatre Chemins profile is an exposure of T3d on the left bank of the Têt (Figs. 2 and 6). Nine multiple-clast samples of quartz gravel (long axis: 1–3 cm) were collected: 3 at the surface, 6 others at increasingly greater depths to 380 cm (Table 1, Fig. 10). The depth–concentration plot reveals a large scatter of TCN values, not just at the surface (as in T3c) but also at depth. This might result from spatially non-uniform geochemical eluviation processes in the alluvial deposit but also from a large scatter in pre-depositional TCN concentrations among individual clasts. As in the case of T3c, the age–denudation plot shows a statistical distribution of [χ^2min; χ^2min+1] best-fitting solutions (n = 6341, blue dots in Fig. 10, Table 2) characteristic of a steady-state profile, again with a wide band of statistically acceptable exposure ages (104.5–999.5 ka) and a narrow band of denudational solutions (0–0.68 cm/ka). The minimum age among the 100,000 model solutions was 93 ka.

5.2. ESR results

Sixteen samples collected from isolated sandy lenses interlayered between the coarser stratigraphic units (Fig. 7c, 9c,d and i) were measured using the ESR multiple centres approach. Given, however, that the Ti signals were in all cases too low to be recorded, all ESR ages from the Têt Pleistocene fluvial sequence are based on Al signal intensities. Moreover, samples 14–01, 14–07 and 14–09 were fruitless because the Al signals measured on the different aliquots were highly scattered. Table 3 presents the results obtained for the 13 remaining samples. Just three of those ages were modelled using the full population of measurement points. In the case of the other 10 samples, age modelling was numerically possible only on condition that one or two outliers were eliminated from the ESR intensity dose growth curve. The analytical quality of those ages is therefore slightly less robust even though the R^2 values still exceed 0.95 (Fig. 11). Such scatter in the dose response of aliquots can be explained by a mix of grains with different provenances and different bleaching histories. The source of some grains is the Axial Zone, whereas others come from more local sources (e.g. Pliocene sand of the Roussillon). Another possibility is the contamination by quartz grains provided by weathered granite or gneiss pebbles. Nevertheless, the ESR ages clarify the data provided by the TCN profiles, and provide a consistent chronological pattern for the sequence of Têt terraces.

5.2.1. Results for T1

Only one sample (14–08) was collected from terrace T1 in a 3- to 4-m-deep gully at Pézilla-la-Rivière (Figs. 2 and 9a-b). The exposure exhibits channels filled with unweathered pebbles of granite and gneiss, and 1 m-thick interlayers or lenses of sand. The model ESR age for this site was obtained from a 7-point fit out of 8 aliquots (Fig. 11). The age is 153 ± 30 ka, suggesting that T1 aggraded during MIS 6 (Fig. 12). This age is suspiciously old given the very low weathering grade of the debris and the low elevation (4–5 m) of the alluvial deposit above the Holocene to modern alluvial plain (T0, which contains a brick- and charcoal-bearing deposit dated to 414–544 cal. ^{14}C yr AD: Lyon-8924, OxA, Fig. 9a–b). Considering further that the ESR method is reported to overestimate burial age in recent deposits in certain circumstances (Voinchet et al., 2015), it is thus likely that T1 is Würmian (MIS 2 or MIS 4) rather than Rissian (MIS 6).

5.2.2. Results for T2

T2 was sampled at the same roadcut exposure as the TCN Escatllars profile (Figs. 2, 6 and 9c). The two ESR ages obtained were 174 ± 44 ka (sample 14–10, 1.8 m depth) and 259 ± 90 ka (sample 14–11, 3 m depth). The uncertainty intervals of these two ages overlap, suggesting an aggradation of T2 during MIS 6 (Fig. 12). The model ESR ages were obtained from 7- and 6-data-point curve fits out of a total of 8 aliquots (Fig. 11). These results are analytically perfectible, but concur with the moderate weathering grade of

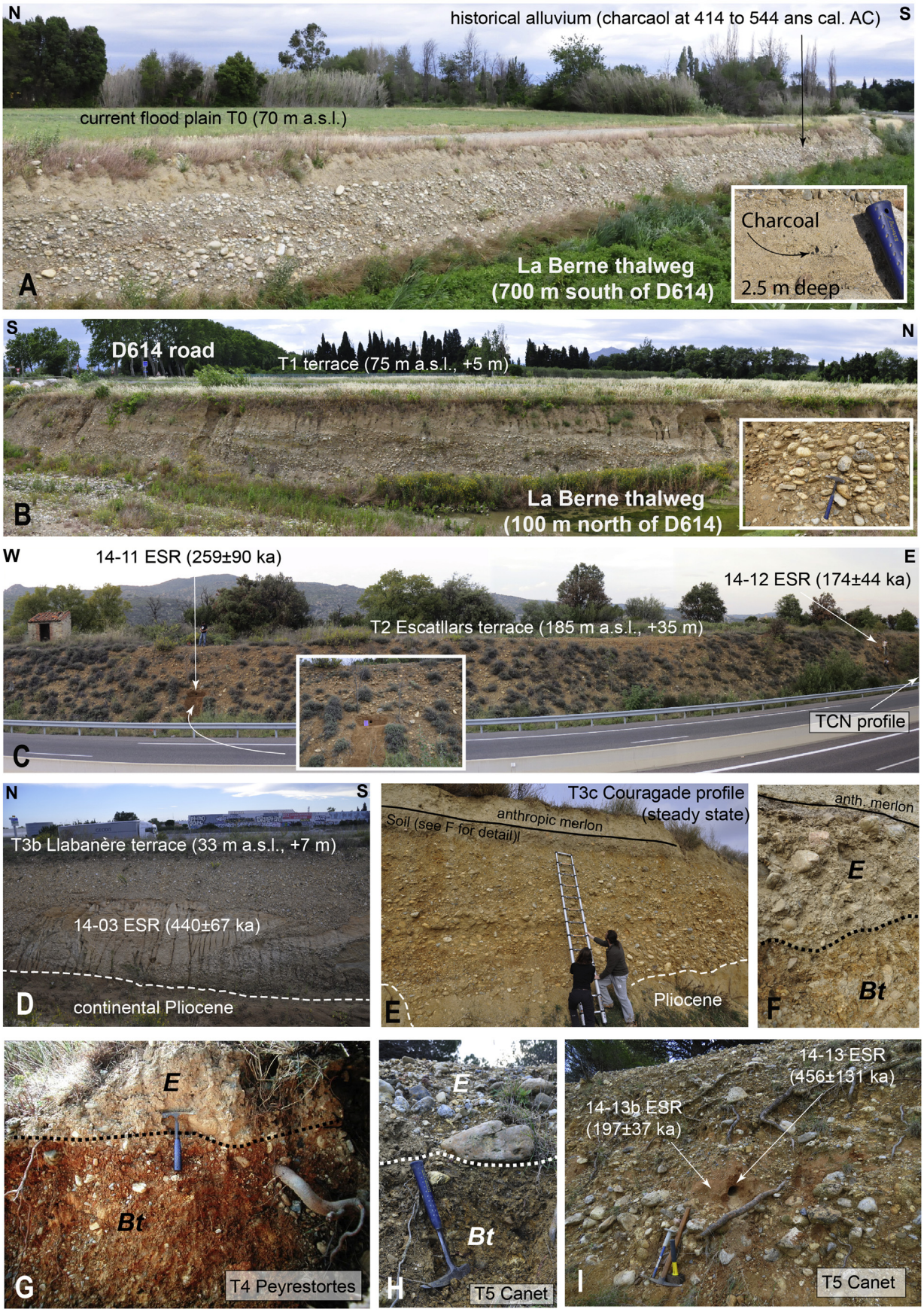

Fig. 9. Sedimentological facies, weathering grade, and soils capping the Têt Pleistocene fluvial sequence.

Table 1
^{10}Be concentrations in the alluvial depth profiles.

Location	Sample code	Depth[a] (cm)	^{10}Be concentration (at/g)	Analytical uncertainty (at/g)
T2 Escatllars	ESC 15-0	0	353464	12081
N 42.658105	ESC 15-1	40	172872	7807
E 2.599817	ESC 15-2	65	106845	5220
Elev. 181 m	ESC 15-3	125	97994	4976
No shielding	ESC 15-4	200	60220	3422
	ESC 15-5	300	no data	no data
	ESC 15-6	475	36220	2760
T3c Couragade	COUR 15-03R	0	652593	22144
N 42.722724	COUR 15-02B	0	546035	17239
E 2.864459	COUR 15-01J	0	1124069	36664
Elev. 50 m	COUR 15-0	0	879724	27214
No shielding	COUR 15-1	50	369131	11646
	COUR 15-2	100	183799	6305
	COUR 15-3	150	249293	8701
	COUR 15-4	200	136303	11280
	COUR 15-5	250	56931	6369
	COUR 15-6	340	74534	3571
T3d Quatre Chemins	4CHE 15-03B	0	536795	17015
N 42.709732	4CHE 15-02G	0	377388	14580
E 2.796459	4CHE 15-01R	0	1157564	39426
Elev. 80 m	4CHE 15-1	45	414673	13150
No shielding	4CHE 15-2	80	193115	12070
	4CHE 15-3	120	369047	19816
	4CHE 15-4	170	76581	5257
	4CHE 15-5	260	201920	6654
	4CHE 15-6	380	66105	6442

[a] Sample depths were measured in the field with a graduated levelling staff.

Table 2
Model outputs for the five depth profiles.

Sampling site	Range of solutions [χ^2min; χ^2min+1]			Ranges of solution constrained by top 100 χ^2min		
	Exposure time (ka)	Denudation (cm/ka)	Inheritance (at/g)	Exposure time (ka)	Denudation (mm/ka)	Inheritance (at/g)
T2-Escatllars	369–976	0.85–0.96	27,967–41,937	323–986	0.85–0.99	22,968–41,937
T3c-Courragade	170–998	0.01–0.42	20–60,722	472–994	0.34–0.39	371–36,513
T3d-Quatre Chemins	104–999	0–0.68	143–144	110–453	0–0.59	73,088–93,409

Table 3
ESR results obtained on quartz extracted from alluvial sediments.

Stratigraphy	Location[a]	Sample code	Water content[b]	δbl[c]	Dose rate[d]	Equivalent dose[e]	R^2	ESR Age
			%	%	(μGy/a±1σ)	(Gy±1σ)		(ka±1σ)
T1	Pézilla	TET 14-08	5	39	4960 ± 74	744 ± 288	0.973	153 ± 30
T2	Escatllars	TET 14-10	7	42	4529 ± 76	787 ± 402	0.937	174 ± 44
		TET 14-11	3	43	5129 ± 67	1259 ± 509	0.938	259 ± 90
T3b	Llabanère	TET 14-02	5	44	4163 ± 73	1528 ± 379	0.986	374 ± 47
		TET 14-03	11	37	4404 ± 67	1883 ± 329	0.994	440 ± 39
T3c	Courragade	TET 14-01	2	No data	3368 ± 52	No data	No data	No data
T3d	Quatre Chemins	TET 14-06	10	34	4635 ± 78	3324 ± 2404	0.98	744 ± 269
		TET 14-07	8	No data	4760 ± 85	No data	No data	No data
T4	Campeils	TET 14-09	4	No data	5006 ± 88	No data	No data	No data
	Peyrestortes	TET 14-04	7	43	4621 ± 76	2889 ± 1692	0.934	637 ± 188
		TET 14-05	6	49	4372 ± 75	2466 ± 771	0.995	582 ± 92
T5	Canet	TET 14-12	6	39	3761 ± 57	3932 ± 3690	0.927	1058 ± 498
		TET 14-13	6	38	3579 ± 62	1610 ± 919	0.976	456 ± 131
		TET 14-13b	6	40	4206 ± 65	799 ± 300	0.956	197 ± 37
	Villefranche	TET 15-01	5	41	4308 ± 39	5732 ± 1605	0.992	1133 ± 159
		TET 15-02	5	36	4544 ± 62	5606 ± 1811	0.987	1099 ± 179

[a] Pézilla: N 42.692476, E 2.749587, 74 m. Escatllars: N 42.658105, E 2.599817, 182 m. Llabanère: N 42.739869, E 2.886891, 32 m. Courragade: N 42.722724, E 2.864459, 50 m. Quatre Chemins: N 42.709732, E 2.796459, 80 m. Campeils: N 42.713462, E 2.718687, 144 m. Peyrestortes: N 42.748433, E 2.848650, 68 m. Canet: N 42.704224, E 3.017510, 13 m. Villefranche: N 42.588953, E 2.362453, 550 m.
[b] Water contents (%) were estimated by the difference in mass between the natural sample and the same sample dried in an oven at 50 °C for a week.
[c] Bleaching rate δbl (%) is determined by comparison between the ESR intensities of the natural and bleached aliquots (δbl= ((Inat-Ibl)/Inat)×100).
[d] Dose rates were determined taking into account alpha and beta attenuations estimated for the selected grain sizes from the tables of Brennan (2003); k-value of 0.15 (Yokoyama et al., 1985).
[e] Equivalent doses were determined from a coupled exponential and linear function using the Microcal OriginPro 8 software and $1/I^2$ weightings.

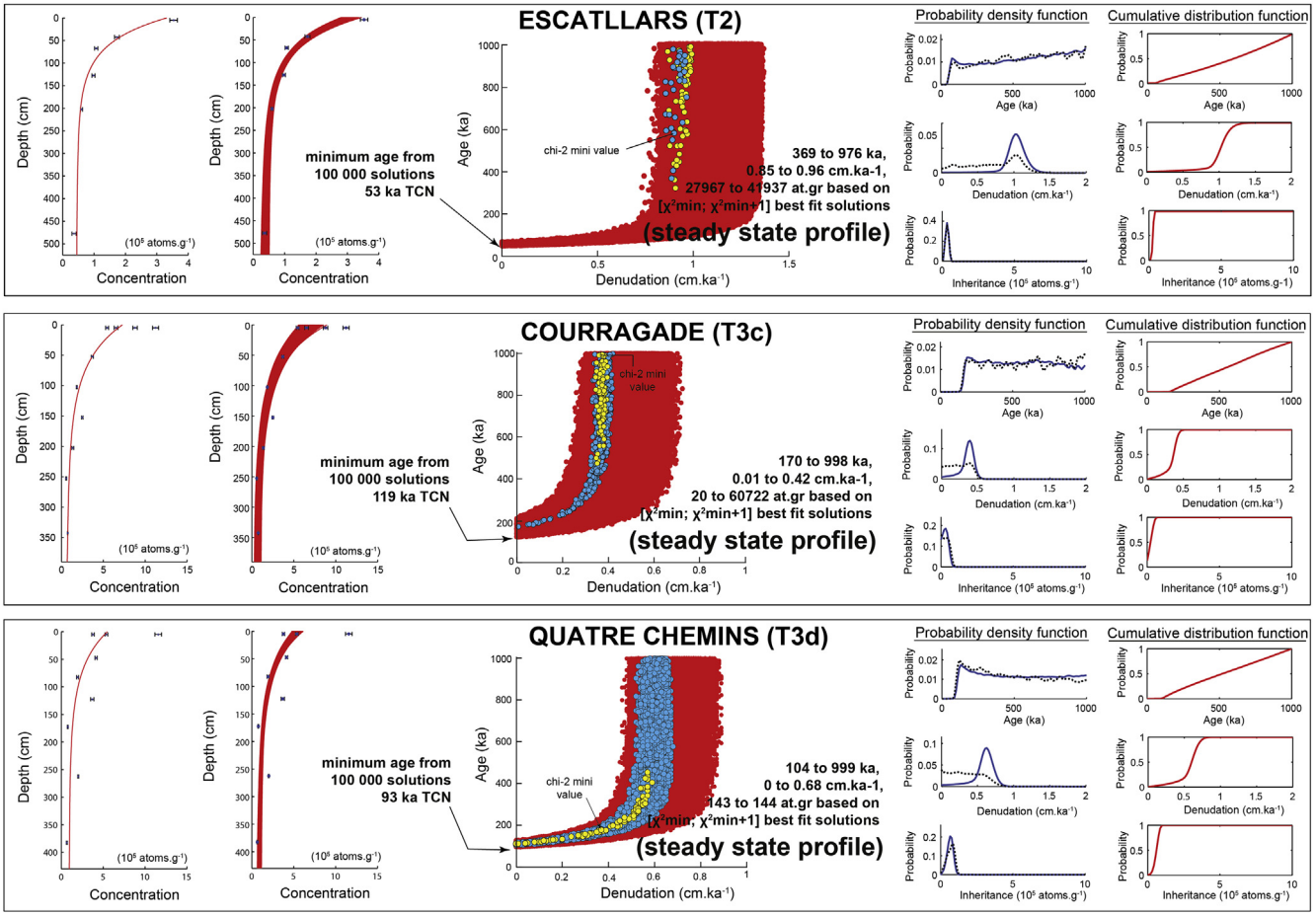

Fig. 10. Depth profiles and age–denudation models for the Escatllars, Courragade and Quatre Chemins terraces. Blue and yellow dots on age–denudation graphs highlight the solutions that match the χ^2 values within the boundaries of [χ^2min; χ^2min+1] and the 100 smallest χ^2 values, respectively. On the right, blue and stippled curves are the probability density functions and minimum χ^2 (smoothed curve), respectively. Graph plotted using the Hidy simulator (Hidy et al., 2010). (For interpretation of the references to colour in this figure legend, the reader is referred to the Web version of this article.)

clasts in the deposit, with features of the topsoil (see section 3.1 and Suppl. Information 1), and with the terrace tread's position 15 m above T1.

5.2.3. Results for T3

Level T3 consists of several isolated alluvial strips upstream of Millas, and of a remarkably continuous tread on the north edge of the Roussillon tectonic basin (Figs. 2 and 6). Farther downstream, e.g. in the vicinity of Perpignan, generation T3 is vertically offset into 4 separate treads spanning an elevation band of ~15 m. The lowest tread, T3a, was not dated because of an absence of suitable exposures. T3b produced two ESR ages. Both are very close 374 ± 47 ka (14–02) and 440 ± 39 ka (14–03), thus indicating a deposit emplacement at the time of MIS 10 or MIS 12. Sample 14–01 from level T3c was fruitless. Level T3d produced only one model ESR age (14–06) out of two samples. The wide uncertainty 744 ± 269 ka covers MIS 14 to MIS 28 (Fig. 12).

Out of the three analytically acceptable ages obtained for T3, the most robust is that obtained for sample 14–02 (374 ± 47 ka, i.e. MIS 10) because it relies on all 8 aliquot results. The other model ages, 440 ± 39 ka (14–03) and 744 ± 269 ka (14–06), omitted one aliquot outlier in each case (Fig. 11). However, and despite the very wide error margin for 14–06, all three ESR age brackets are compatible with the weathering and pedogenetic features characteristic of T3. T3 (and particularly T3b, T3c and T3d, which bear 90 cm-thick clay-rich Alfisols containing up to 80% quartz pebbles: Fig. 9f), exhibits a step change from T2. Based on these criteria, the aggradation of T3b at the time of MIS 10 is entirely plausible; likewise for an aggradation of T3d at the time of MIS 12 or earlier.

5.2.4. Results for T4

T4 was sampled at two locations, but only the Peyrestortes site yielded analytically meaningful results. Two ESR model ages of 637 ± 188 ka (sample 14–04) and 582 ± 92 ka (sample 14–05) were produced from 7 points out of a total of 8 aliquots (Fig. 11). The analytical quality is thus comparable to that of 14–06 on T3d, but uncertainty intervals are narrower (Fig. 12). Furthermore, ages on T4 are consistently older than T2, where the best ESR age (174 ± 44 ka) matches MIS 6; and they are likewise older than T3b, where the best ESR age (374 ± 47 ka) matches MIS 10.

5.2.5. Results for T5

T5 was sampled at two locations: upstream in the gorge at Villefranche-de-Conflent, and downstream near the coast at Canet (Figs. 2, 6 and 7). The two samples from Villefranche yielded good constraints, with ages of 1133 ± 159 ka (sample 15–01, modelled from all the aliquots) and 1099 ± 179 ka (sample 15–02, modelled on the basis of 7/9 points). Another remarkable feature is that these ages concur with ages between 2 and 1 Ma independently obtained from river gravel buried within the Faubourg Cave in the Têt canyon near Villefranche, where the dated alluvium in the cave system lies in perfect topographic alignment with the subaerial outcrop of T5

(Fig. 7; Calvet et al., 2015a).

The Canet site produced two samples from an embankment along route D81. Sample 14–12 was collected from a lens of red sand containing large numbers of small pebbles, all friable to the core. The irradiation–ESR intensity plot shows a large scatter of data points likely related to the occurrence in the sand fraction of quartz grains released from granitic debris that had undergone intense granular weathering in the profile (Fig. 9h–i and 11). The inference is thus that quartz crystals released from weathered granite pebbles and quartz grain concentrations in the sand lenses of the alluvial deposit displayed different bleaching signatures. One model age was nonetheless produced from 6 out of 8 aliquots with a moderately good fit ($R^2 = 0.927$), which explains the wide uncertainty around the central age of 1058 ± 498 ka. The Canet deposit was sampled at a second location ca. 20 m to the south of the sample 14–12, with an uptake of identical materials as in 14–12. The two model ages (samples 14–13 and 14-13b) obtained from this same sample (Fig. 9i), are analytically robust but yielded highly contrasting ages, with no overlap between their uncertainty intervals: 456 ± 131 ka in the case of 14–13 (modelled on the basis of 8/8 points), and 197 ± 37 ka in the case of 14–13b (modelled on the basis of 7/8 points, Fig. 9i). Retaining the age modelled on the basis of 8/8 points (i.e. 14–13 at 456 ± 131 ka) would call for ascribing the Canet terrace to one of the T3 or T4 topographic benches located on the left bank of the Têt River (Figs. 2 and 6). This hypothesis, however, would imply a +30 m post-T3 (or +10 m post-T4) tectonic uplift of the SE block when actually the sense of fault slip — based on tectonic indicators in the underlying Pliocene beds — indicates the reverse (Fig. 8, Duvail et al., 2001). An alternative interpretation would consist in envisaging that terraces T4 and T5 are indistinguishable near the coastline and that, as a consequence, the ESR age of 456 ± 131 ka obtained at Canet dates the aggradation of T4, not of T5. The bottom line is that neither of the two ESR ages (samples 14–13 and 14-13b) obtained from the same sand unit (Fig. 9i) are reproducible. It is therefore preferable to reject the ESR results obtained for T5 at Canet and rely instead on the more robust ages obtained for T5 at Villefranche — i.e. in the upstream part of the watershed.

6. Discussion

6.1. Summary of TCN and ESR results obtained from the Têt watershed

Two terrace levels, T3b and T5, obtained robust age constraints at 374 ± 47 ka (14–02) and 1099 ± 179 ka (15–02) from ESR data of excellent analytical quality (sample 14–02 was modelled on the basis of 8/8 points and 15–02 on the basis of 9/9 points). These results place the aggradation of alluvial unit T3b at the time of MIS 10, and of unit T5 before the Early to Middle Pleistocene transition and the onset of the 100 ka climatic cycles (Head and Gibbard, 2015). The analytical quality of the 174 ± 44 ka ESR age obtained for T2 at Escatllars is slightly less robust (sample 14-10 modelled on the basis of 7/8 points). However, the strong consistency of this age with the weathering grade of the deposit, with its soil characteristics, and with the position of T2 in the terrace sequence (see section 3.1, Figs. 5–8) places the aggradation of T2 during MIS 6.

The ESR and TCN ages obtained for other generations of terraces are more equivocal. The TCN profile obtained for T3c at Courragade indicates a minimum age of 170 ka (i.e. MIS 6) even though T3c is stratigraphically older than T3b (which was accurately ESR-dated and correlates with MIS 10). The wide uncertainties obtained for T3d (Quatre Chemins) and T4 (Peyrestortes) preclude any clear correlation with global marine stages. Lastly, the correlation of terrace T1 with the Würm is consistent with the very low weathering grade of the debris, the youthfulness of soil profiles, and the topographic position of the tread just above the modern floodplain. The ESR age obtained at Pézilla for T1 (sample 14–08: 153 ± 30 ka) is therefore considered spurious until further dating efforts are undertaken.

6.2. Regional correlation across SW Europe

Results for the Têt watershed coincide quite well with the regional data obtained from other fluvial terrace sequences on both sides of the Pyrenees (Fig. 13; Cordier et al., 2017) and more widely in Languedoc and in the Iberian Peninsula (Duero watershed, in particular).

6.2.1. The highest terraces T5 and T4

The early Pleistocene ages in excess of 1 Ma obtained on the Têt River for T5-Fu correlate remarkably well with the highest known terrace of the Hérault River in Languedoc, which was given a minimum age based on the 1.6–1 Ma age of basalt flows capping the alluvium. This period predates valley incision on the southern edge of the Massif Central (Ambert, 1994; Bourguignon et al., 2015, 2016). The age bracket is also consistent with the uppermost terraces of the Alcanadre watershed, which joins the Cinca River in the central Spanish Pyrenees. It yielded an ESR age of 1276 ± 104 ka and palaeomagnetic data consistent with the ESR age (Calle et al., 2013; Sancho et al., 2016). It is likewise consistent with the 1.14 ± 0.13 Ma ESR age obtained for the lowest (T3azn) among three high-level terraces of the Arlanzón River, which joins the Atlantic drainage of the Duero (Moreno et al., 2012).

The 300 ka TCN exposure age obtained from the Lannemezan megafan surface (Mouchené et al., 2017), which regionally occupies the stratigraphic position of terrace T5 along the northern mountain front of the Pyrenees, is a minimum age. This open-ended constraint arises because the age was not obtained from a vertical profile but is instead an isolated sample (sample LAN3) modelled as an exposure age under the assumption of no post-depositional surface erosion. This assumption is highly debatable because the Lannemezan fan exhibits many signs of substantial (but unquantified) post-depositional denudation. The 300 ka minimum age is thus almost certainly much less that the true depositional age of the Lannemezan megafan, which actually consists of two alluvial formations — both deeply weathered (Icole, 1974; Hubschman, 1975d) and dissected by networks of shallow valleys and interfluves. Importantly, these highly weathered, siliciclastic deposits forming the main mass of the megafan form a stratigraphic continuum northward with similar (but finer-textured) formations on the Landes Plateau (Dubreuilh et al., 1995). In the Landes, palynostratigraphic and macrofloral indicators contained in lignite interlayers, which occur throughout the fluvial sequence, have provided chronostratigraphic constraints on the Pliocene to Quaternary transition from the lowermost Arengosse Formation (Pliocene) upward through the Onesse to the Beliet Formation (Lower Pleistocene), which caps the 70-m-thick alluvial sequence. The Belin Formation (10–20 m thick) is attributed to an ancestral Garonne River with its floodplain sequence inset in the stack of older formations (synthesis in Dubreuilh et al., 1995, Fig. 1a).

Terrace T4-Fv on the Têt River is more difficult to correlate with other dated fluvial levels in SW Europe: it could be coeval with the Hérault alluvial beds covered by volcanic rocks, $^{39}Ar/^{40}Ar$-dated to 680 ka at St Thibéry (Ambert, 1994; Bourguignon et al., 2015, 2016), and with terraces T4azn or T5azn on the Arlanzón River, where ages

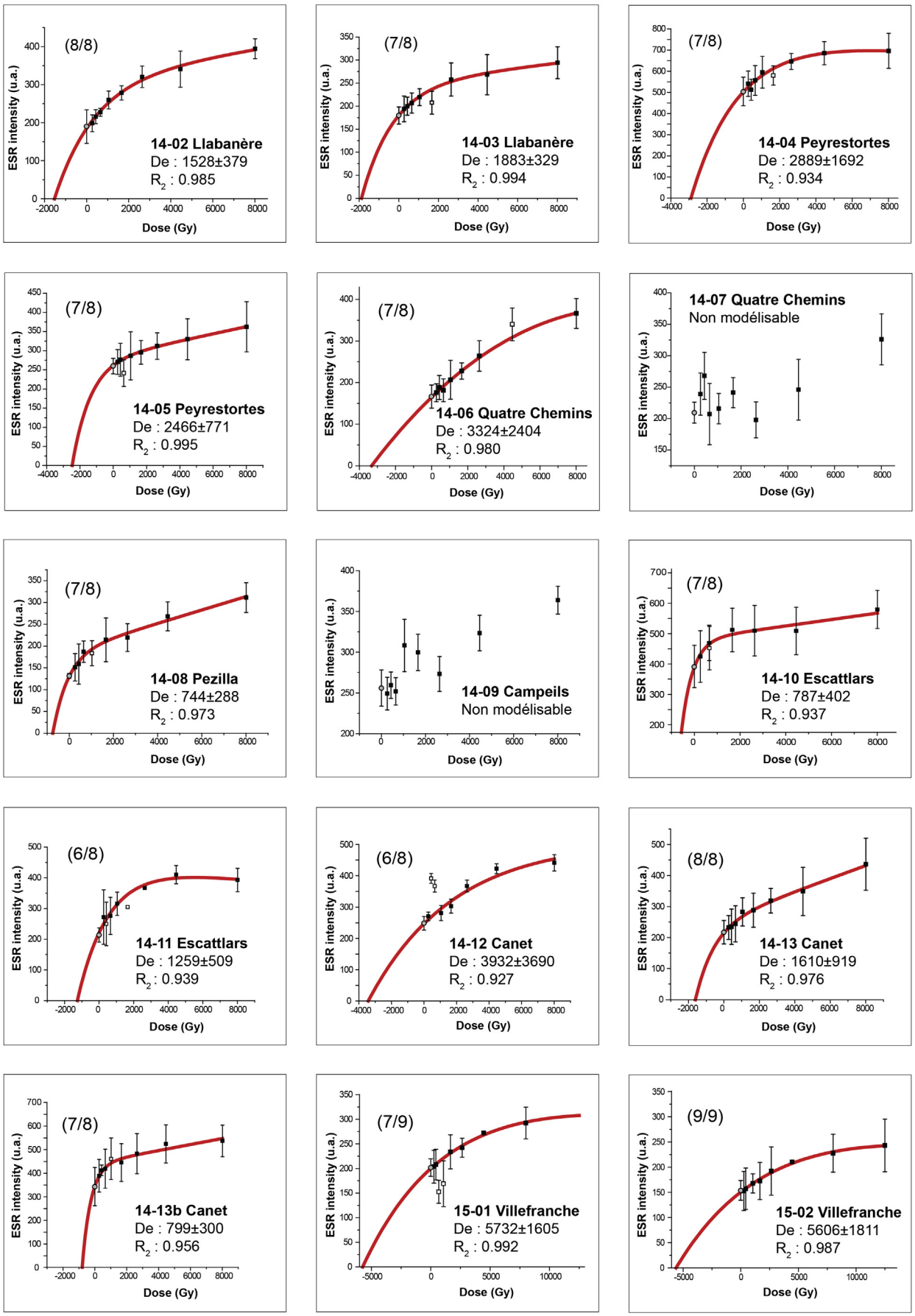

Fig. 11. ESR signal dose response curve for each sample. Black squares were used in age calculation models; white squares represent the excluded data points (outliers). Grey circle represent the geological dose.

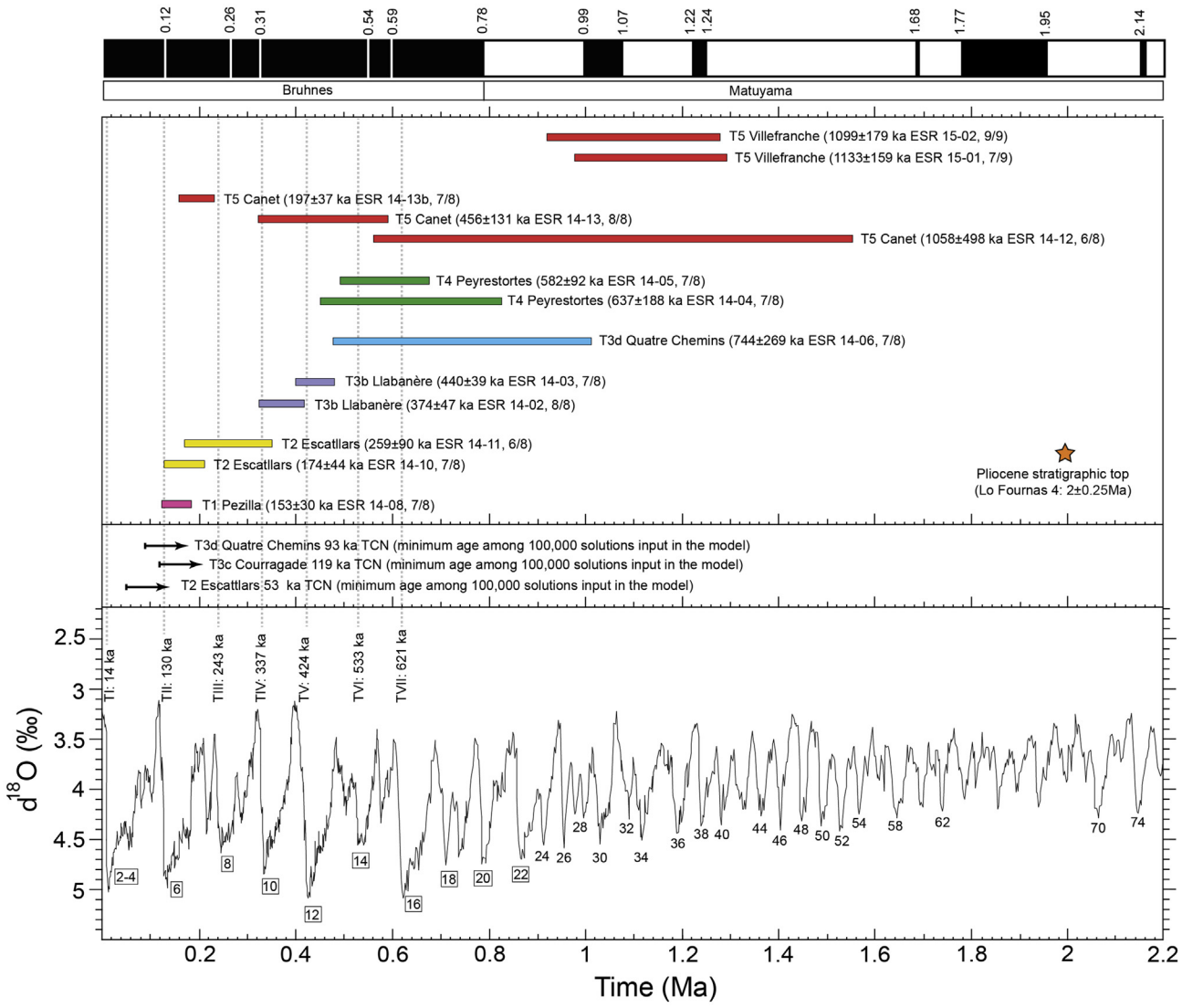

Fig. 12. Tentative correlation between dating of the Têt Pleistocene fluvial sequence and the global marine isotopic curve of Lisiecki and Raymo (2005).

of 0.78 ± 0.12 Ma to 0.93 ± 0.10 Ma for T4azn; and 0.70 ± 0.10 Ma to 0.70 ± 0.07 Ma and 0.60 ± 0.11 Ma for T5azn are reported (Moreno et al., 2012). On the north-Pyrenean retro-foreland, level T4 is poorly developed in the Ariège watershed (Delmas et al., 2015) but better represented in the Garonne–Neste (high level at Labarthe-de-Neste; Rieumes terrace) and along the Gave de Pau (Morlaas palaeovalley and its two deeply weathered and slightly offset alluvial units, noted Fu2-Fv or Fv2-Fv3 depending on the geological map: Barrère et al., 2009). Unit Fv2 is covered by loess layers each separated by rubified paleosols (Btg horizons). The lower sandy quartz layers of these stratigraphic sequences have produced luminescence ages ranging between 189 ± 13 and 348 ± 22 ka upstream, and between 168 ± 12 and 317 ± 23 ka downstream of Aire-sur-l'Adour (Hernandez et al., 2012). On the south-Pyrenean foreland, a greater abundance of elevated terrace levels has been reported than in the northern Pyrenees, but correlations from one Ebro tributary to another are often unclear. In the Cinca watershed, where 10 levels have been identified in total, only the two most elevated terraces (Qt1 and Qt2) are older than the Brunhes–Matuyama reversal, i.e. older than 781 ka (Lewis et al., 2009, 2017). On the Gállego, with 12 tread levels in the downstream region, the six most elevated terraces (T06 to T01) are also reportedly older than 781 ka (Benito et al., 1998, 2010). Any correlation at this stage between one of these high levels and level T4 in the Têt watershed would be premature.

6.2.2. *The population of intermediate and lower terraces*

Regional correlation becomes increasingly difficult as we descend into the lower tiers of the sequence.

6.2.2.1. Correlations with the terrace sequences of the Aquitaine piedmont zone. A relatively consistent scheme can be established in the north-Pyrenean retro-foreland basin, where the weathering chronosequences are spatially quite uniform owing to clastic input predominantly from crystalline source areas. For example, in the Ariège watershed two vertical TCN profiles (Tournac and Château de Fiche) presenting the characteristics of a nuclide steady state situation produced minimum ages of 60–145 ka for T2 and 204–226 ka for T3, thus allowing a correlation of T2 with MIS 6 ant T3 with MIS 8 (Delmas et al., 2015). Significantly, generation T3 displays both on the Ariège and on the Têt at least 3 separate terrace treads (the Château de Fiche site being the lowest). Similarly, the three vertical TCN profiles on T1 in the Ariège watershed provided terrace ages of 19.5–14 ka (Montgaillard profile),

17.4–13.4 (Filatier profile) and 16.5–12.5 ka (Cintegabelle profile). These ages for T1 on the Ariège concur with TCN ages on the lower terrace of the Garonne River ($14^{+9.6}_{-4.3}$ ka at Rivières and $13^{+6.7}_{-3.9}$ ka at Cazères, Stange et al., 2014), as well as on the Neste River at Bizous (21^{+4}_{-5} ka, Mouchené et al., 2017). A similar TCN age (18 ± 2 ka) was reported from the top of the thick alluvial sequence of Gurmençon on the Gave d'Aspe, farther west along the north-Pyrenean mountain front (Nivière et al., 2016). Lastly, for the middle terrace T3, two TCN ages of 121^{+52}_{-30} (GAU profile) and 95^{+14}_{-23} ka (ESC profile) were produced for the Garonne River at Saint-Gaudens (Mouchené et al., 2017).

In the case of T3 on the Garonne, obtaining such young ages for such deeply weathered and intensely rubified alluvium — whether at Saint-Gaudens or farther downstream at Léguevin-Saint-Lys (Hubschman, 1975a; b; c) — appears spuriously anomalous. Accordingly, we remodelled the GAU profile of Mouchené et al. (2017) while applying the same model constraints as for the vertical profiles in the Têt valley (this study) — i.e. no input constraints on any of the key parameters, and by letting the model search for age and denudation-rate solutions within much wider bands (0–1 Ma, and 0–2 cm/ka) than Mouchené et al. (2017) (who restricted their model space to 0–300 ka and 0–1 cm/ka). Modelling results yielded a single acceptable age–denudation solution at 220 ka and 0.028 cm/ka falling within the [χ^2min; χ^2min+1] interval. The solutions among the 100 best χ^2 scores indicated exposure ages ranging between 200 and 613 ka, and denudation rates between 0.002 and 0.3 cm/ka (Suppl. Information 4). On this revised basis, the values obtained become compatible with the TCN ages obtained for T3 on the Ariège (Delmas et al., 2015), and also with the regionally consistent weathering attributes of this generation of deposits. In contrast to the GAU profile, remodelling the other profiles of the Neste River based on the same principles attained a good reproducibility of the ages published by Mouchené et al. (2017), i.e. 88–128 ka for T3 (ESC profile — a natural exposure poorly suited to the requirements of the TCN profile sampling approach; see Mouchené et al., 2017, Fig. 6 therein), 15.7–20.8 ka for T1 (Bizous profile), and 0.15–1.2 ka for Tuzaguet, which is actually located in the Holocene floodplain.

In the Ariège watershed, age remodelling of the three TCN profiles on T1 while using the parameter settings favoured in this study yielded results that were similar to those originally published, i.e. 14.3–22.8 ka for the Montgaillard profile, 13.1–18.9 ka for the Filatier profile, and 11.3–20.6 ka for the Cintegabelle profile. In the same way, the new models confirm that the Tournac and Château de Fiche TCN profiles have reached a nuclide steady state and thus provide only minimum ages (Suppl. Information 5).

6.2.2.2. Correlations with the terrace sequences of the Ebro piedmont zone. In the Ebro Basin, TCN ages published for the middle terraces of the Segre and the Noguera Ribagorzana ($202^{+35.3}_{-32.9}$ ka for TQ1 and $138.8^{+46.7}_{-22.8}$ ka for TQ2), which occur respectively at +100–118 m and +77–88 m above the modern river channels (Stange et al., 2013), could appear prima facie rather young given that the highest level TQ0 lies only 50 m above those two (note the reverse order of terrace notation in Spain compared to France, where terrace numbers increase rather than decrease with age, Fig. 13). Yet these TCN age brackets seem confirmed by the 178 ka OSL age obtained for terrace Qt5 on the Cinca River at +80 m (Lewis et al., 2009), i.e. midway up the terrace sequence as in the Segre watershed. Terrace levels attributed to MIS 6 on the Gállego River, with 6 OSL ages

	NORTH-PYRENEAN WATERSHEDS			SOUTH-PYRENEAN WATERSHEDS				
Time	**Aspe/Ossau/ Pau**	**Garonne/Neste**	**Ariège**	**Valira/Segre/ N. Ribagorzana**	**Cinca/ Alcanadre**	**Upper Gállego**	**Lower Gállego**	**Upper Aragón**
Upper Pleistocene	Aspe T1 «Gurmençon» +40 m at Gurmençon (Outer fold belts) 18±2 ka TCN Ossau T1 «Ogeu» +30 m at Oloron (Foothill zone)	Garonne T1 «Basse plaine» +14 m at Rivière +25 m at Cazères (Foothill zone) Rivière,14.6 $^{+9.6}_{-4.3}$ ka TCN Cazères, 13 $^{+6.7}_{-3.9}$ ka TCN Neste Fxa (T1/2?) +25 m at Château de Boucoulan +30 m at Bizous (Outer fold belts) Bizous, 21 $^{+4}_{-5}$ ka TCN	T1 «Grausse de Pamiers» +45 m at Montgaillard (Outer fold belts) +20 m at Filatier +15 m at Cintegabelle (Foothill zone) Montgaillard,17.5 $^{+2.0}_{-3.5}$ka TCN Filatier,13.8 $^{+3.6}_{-0.4}$ka TCN Cintegabelle, 13 $^{+3.5}_{-0.5}$ka TCN	TQ7, +3 to +5 m* (Foothill zone) TQ6, +8 to +14 m* (Foothill zone) SVT8/T9, +8 to +10 m* (Axial Zone) 32.8±1.2 ka OSL TQ5,+16 to +26* m (Foothill zone) SVT7, +15 m (Axial Zone) TQ4,+35 to +47* m (Foothill zone) 61.8 $^{+4.6}_{-5.4}$ ka TCN TQ3,+48 to +65* m (Foothill zone) 99.6 $^{+31}_{-19}$ ka TCN	Qt9, +6 to +10 m* 11±1 ka OSL (Foothill zone) 15.2±0.1 ka BP ^{14}C 22.1±0.2 ka BP ^{14}C (Outer fold belts) Qt8, +20 m (Foothill zone) 47±4 ka and 51±4 ka OSL Qt7, +35 to +50 m* (Foothill zone) 61±4 ka OSL Qt6, +60 m (Foothill zone) 97±16 ka OSL	«Lower terrace» +5 m at La Peña +45 m at Murillo +35 m at Biscarrues (Outer fold belts) 32±4 ka OSL upstream 45±3 ka OSL «Middle terrace» +11 to +17 m around la Peña (Outer fold belts) 68±7 ka OSL 103±7 ka OSL	(All data on foothill zone) T12, +3 to +10 m* 16.8±1.3 ka OSL T11, +10 to +12 m* 55.4±7.4 ka OSL 54.4±8.8 ka OSL T10, +20 m 124±13 ka OSL 110±20 ka OSL	(All data on outer fold belts) «20 m terrace» 68±7 ka OSL
Middle Pleistocene	Aspe T2 «Agnos» +60 m at Agnos (Outer fold belts) Ossau T2 «Herrères» +50 m at Oloron (Outer fold belts) T3 Pau T4 «Fu-v ou Fv1-2» Morlaas palaeo-valley + 130 m at Andouins (Foothill zone) OSL ages on aeolian silts on Fv2 level 189±13 ka OSL 348±22 ka OSL Upstream of Aire-sur-Adour 168±12 ka OSL 317±23 ka OSL downstr. of Aire-sur-Adour	T2 «basse terrasse» «Blagnac-Seysse» +35 m at Cazères +25 m at Seysse +25 m at Blagnac (Foothill zone) T3 «moyenne terrasse» «StGaudens-Montréjeau» +65 m at Labarthe-de-Neste +55 m at Montréjeau +50 m at St Gaudens (Foothill zone) St Gaudens, 121 $^{+52}_{-30}$ ka TCN Escala, 95 $^{+14}_{-23}$ ka TCN T3 «moyenne terrasse» «Léguevin-St Lys» +75 m at Bérat, +55 m at St Lys +60 m at Léguevin (Foothill zone) T4 «haute terrasse» «Rieumes» +115 m at Rieumes +100 m at Léguevin (Foothill zone)	T2 «Basse Boulbonne» +45 m at Tournac + 30 m at Château de Fiche +30 m at Montaut (Foothill zone) Tournac, 60-145 ka TCN (minimum age) T3 «Haute Boulbonne» +55 m at Château de Fiche +65 m at Montaut (Foothill zone) Ch.Fiche, 204-226 ka TCN (minimum age) T4 +75 m at La Treyte-Coussa (Foothill zone)	SV-T5, +40 m (Axial Zone) 125±11 ka OSL 120±15 ka OSL TQ2,+77 to +88 m* (Foothill zone) 138.8 $^{+46.7}_{-22.8}$ ka TCN TQ1,+100 to 118 m* (Foothill zone) 202 $^{+35.3}_{-32.9}$ ka TCN SVT3/SVT4, +105 m (Outer fold belts) SV-T2, +80 m (Axial Zone) ?	Qt5, +80 m (Foothill zone) 178±21 ka OSL Qt4, +85 m (Foothill zone) at Albalate de Cinca Qt3, +105 m (Foothill zone) at Albalate de Cinca B/M (750 ka) Qt2, +130 m (Foothill zone) at Albalate de Cinca	«Upper terrace» +51 m at Sabiñanigo (Outer fold belts) +72 m at Concilio +46 m at Gurrea (Foothill zone) 151±11 ka OSL	T09, +30 to +40 m* 147±16 ka OSL 133±10 ka OSL 163±22 ka OSL 181±13 ka OSL 156±26 ka OSL T08, +45 m T07 B/M (750ka) T06, +60 m T05, +75 m T04, +85 m T03, +95 m	«60 m terrace» 263±4.8 ka OSL
Lower Pleistocene -Pliocene	T5/Ossau megafan top +185 m above the Nez river (Foothill zone) T5/Ger megafan top +150 m at Ossun (Foothill zone)	T5 «Très haute terrasse» «Hte Bouconne, cailloutis de Lomagne» +145 m at Léguevin/Belloc +170 m at Lahage/Rieumes (Foothill zone) Lanemezan megafan +150 m above the Neste River at Lortet (megafan apex) +115 m above the Garonne river at Tourelles/Montréjeau 300 ka TCN (minimum age)	Lannemezan-high gravel on plateaus +190 m at Pauly, near Pamiers (Foothill zone)	TQ0, +172, +155 and +142 m* (Foothill zone) SVT1, +140 to +170 m* (Axial Zone) ?	Qt1, +200 m on right side +247 m on left side at Albalate de Cinca (Foothill zone) Alcanadre Qt1, +160 m 1276±104 ka ESR Reverse paleomag.		T02, +105 m T01	
Ref.	Nivière et al., 2016 Hernandez et al., 2012 Hubschman, 1984	Stange et al., 2014 Mouchené et al., 2017 Hubschmann, 1973, 1975a,b,c	Delmas et al., 2015 Hubschmann, 1975a,b,c	Stange et al., 2013 (TQ) Turu et al. 2016 (SVT) Pena et al., 2011 (SVT)	Lewis et al., 2009, 2017 Sancho et al., 2016	Lewis et al., 2009	Benito et al., 2010	Garcia Ruiz et al., 2013

* depending on location
All TCN data are depth profile ages, except the 300 ka results for the Lannemezan megafan in the Neste valley (see text for details).

Fig. 13. Stratigraphical correlation between Pyrenean fluvial terrace systems García-Ruiz et al., 2013; Peña Monné et al., 2011; Turu et al., 2016.

ranging from 181 ± 13 and 133 ± 10 ka, refer to a system displaying much less relative relief (30–50 m) between the treads of the different terraces (Lewis et al., 2009, 2017; Benito et al., 2010). Finally, the lower terraces form between 2 and 6 strath terraces distributed within a band of relative relief ranging between 20 and 60 m (Fig. 13), with a spread of OSL, occasionally TCN, and ^{14}C ages spanning much of the Würm. The flagship event recorded in all 4 valleys (Segre, Gallégo, Cinca, and Noguera Ribagorzana) coincides with MIS 4. MIS 3 is also detected in three of the four valleys. The Global LGM and Lateglacial, in contrast, are only recorded on the Cinca (Qt9) and the lower Gállego (T12) (OSL and ^{14}C dating).

As with the Garonne and Ariège, we remodelled the TCN profiles of Stange et al. (2013) on the Segre River using the same model parameter space as for the Têt (i.e. permitting the model to randomly enter age inputs between 0 and 1 Ma and denudation inputs between 0 and 2 cm/ka, Suppl. Information 6). The results produced wider uncertainty intervals than originally obtained by Stange et al. (2013), but the best-fit values (with χ^2 falling within the [χ^2min; χ^2min+1] bracket) were more consistent with the regional stratigraphy (Fig. 13). Exposure ages for TQ1 fell between 153 and 668 ka (denudation: 0.04–0.54 cm/ka), for TQ3 between 101 and 180 ka (denudation: 0.06–0.45 cm/ka), and for TQ4 between 127 and 260 ka (denudation: 0.97–1.31 cm/ka). TQ2 was in a nuclide steady state. Based on these results it is likely that the three terrace levels along the Segre River are coeval with T3 and T2 in the Têt watershed.

6.3. Quaternary valley incision rates by the Têt River in a broader Pyrenean perspective

6.3.1. Incision rates over time intervals greater than the quaternary

Like glacial denudation rates (Delmas et al., 2009), valley incision rates depend on the time span over which they are averaged (Finnegan et al., 2014). Given the long time scales considered in this study, the distorting influence of the Sadler effect on equating valley incision with rock uplift (Gallen et al., 2015) are relatively negligible. Here we can estimate accordingly that incision by the Têt River since 6 Ma beneath the Plateau de la Perche (presented in section 2.3) occurred at a mean rate of 53–88 mm/ka depending on the available stratigraphic datum used (+320 m at Planès, +530 m downstream of Fontpédrouse; Fig. 4a,b,d and 5). At Villefranche, the cave of Notre-Dame de Vie (+265 m), which contains alluvium dated between 4 and 5 Ma (Calvet et al., 2015a), suggests incision rates of 53–66 mm/ka. In the Roussillon Basin, incision into the Pliocene sequence, which according to the micromammalian fossil assemblages preserved in limestone surface fissures began ca. 2 Ma (+120 m on the cross-profile in Fig. 8, given further a probable elevation of 160 m a.s.l. for the top of the continental Pliocene in this area), proceeded at a calculated rate of 60 mm/ka. As demonstrated by alluvium burial ages in the vertical cave sequence at Villefranche (Calvet et al., 2015a), incision rates accelerated during the Quaternary. When using T5 (1.1 Ma at Villefranche) as the upper topographic benchmark and the present-day channel elevation as the lower reference level, it appears clearly that vertical incision rates were greater in the upstream than in the downstream reaches: e.g. 60 mm/ka at Baixas (T5: +66 m), 98 mm/ka at Ille-sur-Têt (T5: +108 m), 109 mm/ka at Villefranche (T5: +120 m), and 113 mm/ka at Joncet (T5: +125 m). The highest rate (206 mm/ka) was inferred to occur at the locality of Fontpédrouse, where a residual strath corresponding to T4 or T5 lies at +236 m above the modern stream channel (Figs. 4d and 7).

These incision rates are of the same order of magnitude as across the entire northern and southern piedmont belts of the Pyrenees (Fig. 13), where incision can be estimated from the top of the foreland megafans by using the ESR age of 1.2 Ma obtained for the oldest terrace of the Alcanadre River (a tributary of the Cinca River, Fig. 13; Sancho et al., 2016) and extrapolating it on the basis of the stratigraphic correlations detailed in Section 6.2.1 — i.e. the hypothesis that the most elevated Quaternary alluvial formations encountered in the watersheds of the Pyrenees (Alcanadre, Ger, Lannemezan, terrace T5 on the Têt, etc.) are roughly coeval. On that basis, the highest rates occur on the southern piedmont, probably because of the greater crustal uplift rate of the Ebro foreland compared to the Aquitaine retro-foreland: 205.8 mm/ka in the Cinca (+247 m: Qt1), and 145.8 mm/ka in the Noguera Ribagorzana (+172 m: TQ0). In the Axial Zone at La Seu d'Urgell, the highest terrace level on the Segre River (SVT1: +170 m) provides an incision rate of 140.8 mm/ka. On the north side of the Pyrenees, incision rates on the Garonne River range from 95.8 mm/ka at Toureilles/Montréjeau (+115 m) to 141.6 mm/ka near Toulouse (+170 m at Lahage/Rieumes). Incision values are 129, 125 and 154 mm/ka at the apex of the Lannemezan (+155 m at Lortet), Ger (+150 m at Ossun), and Ossau (+185 m above the Nez River channel) alluvial megafans, respectively.

6.3.2. Acceleration of valley incision since the Middle Pleistocene

Over a period encompassing the last two glacial–interglacial cycles, based on the elevation differences between the tread of T2 and the modern channel and using the most precise ESR age obtained for T2 on the Têt (174 ± 44 ka), the rate of valley incision increased by 60–100% between Perpignan and Olette compared to the earlier periods of the Quaternary (section 6.3.1) (Fig. 5). This increase is not uniform throughout the watershed, as evidenced by the values of 91 mm/ka at Perpignan–St Charles (+16 m), 143 mm/ka at Millas (+25 m), reaching a peak just below the gorge knickpoint at Rodès: 218 mm/ka just above Ille-sur-Têt (+38 m at Escatllars), but 275 mm/ka at the mouth of the gorge cut in granitic bedrock (+48 m). In the Prades basin, and as far upstream as Joncet, rates fell relatively to 189 and 178 mm/ka (where T2 occurs at +33 and + 31 m, respectively). Continuing upstream, the gradient of T2 subsequently steepens sharply near Olette (Figs. 5 and 7), with MIS 6 and younger incision rates rising from 206 to 298 mm/ka downstream (+36 m) and upstream (+51 m) of that locality, respectively.

Maxima are reached at Thuès (+94 m; 540 mm/ka) and Fontpédrouse (+93 m; 534 mm/ka). Along this stream segment, the T2 alluvial deposits are continuous and anomalously thick (45 m) compared to anywhere else in the Têt watershed. However, when restricting measurements to just bedrock incision instead of considering total valley incision, values attain 252–287 mm/ka, i.e. barely more than total values measured at Olette, where the alluvial thickness never exceeds 5–10 m. The major anomaly above the Thuès gorge thus owes more to the aggradation of T2 than to real bedrock incision of the valley itself (Fig. 7a).

The Ariège piedmont also records a fairly recent Quaternary acceleration of valley incision (Delmas et al., 2015). The Pamiers basin records 160 mm/ka of incision below the Lannemezan megafan envelope surface (+190 m at Pauly, based on the strong likelihood that the 1.2 Ma ESR age obtained on the Alcanadre higher fluvial terrace is also valid for the Lannemezan until further evidence is obtained from direct dating: see sections 6.2.1, 6.3.1, and Fig. 13); 220 mm/ka below T3 (MIS 8, ca. 250 ka, +55 m at Château de Fiche); and 200 mm/ka below T2 (MIS 6, ca. 150 ka, +30 m at Château de Fiche). Similar conclusions can be drawn from the southern piedmont zone of the Pyrenees, with records for the Cinca River (449 mm/ka below Qt5, +80 m; OSL at 178 ka by Lewis et al., 2009, 2017) and for the Segre (633 mm/ka below TQ2, +88 m; 139 ka by Stange et al., 2013). Rates inferred for the upper Gállego ("Upper terrace", +46–72 m; ~150 ka OSL, Lewis et al., 2009; Benito et al., 2010) remain lower (306–480 mm/ka).

6.4. The Têt fluvial sequence as a tool for quantifying quaternary neotectonics

6.4.1. Quaternary tectonic uplift in the Axial Zone of the Pyrenees

The key features for evidencing differential tectonic deformation along the east–west strike of the eastern Pyrenees are the progressive fanning pattern of the Têt fluvial terraces from a hinge zone near the modern coastline westward into the mountain range, which contrasts with the normal stratigraphy of Quaternary fluvial deposits on the continental shelf (section 3.2). The geometry of this pattern implies uptilting of the entire Têt watershed during the Quaternary. The stratigraphic boundary between the marine and continental system tracts in the Pliocene sequence of the Roussillon Basin (Figs. 5 and 6), which is also tilted in the same direction as the Quaternary terraces but at a steeper angle, confirms the inference of Quaternary tectonic uplift and provides an additional tool for quantifying its magnitude. This key stratigraphic benchmark occurs at −200 m in the Canet borehole and at +280 at Vinça, which lie 38.7 km apart. When extended to the Col de la Perche, i.e. by another 40.2 km, this mean gradient of 1.24% suggest a minimum magnitude of vertical uplift at the Col de la Perche of ~778 m (or ~764 m along a straight line from Canet to La Perche) in the last 5.33 Ma, thus situating the palaeoelevation of La Perche at ~803–817 m at the beginning of the Pliocene (versus 1581 m at present, Fig. 4a). The uptilt magnitude is taken as a minimum because, in the foregoing calculation, we assumed that the marine to continental Pliocene boundary was initially a stratigraphically horizontal timeline, whereas it actually was a diachronous (coastward-younging) feature. Part of the uplift occurred of course at the time of Pliocene sedimentation, but the peak of uplift occurred during the build-up of the Pleistocene offshore sediment wedge (i.e. 2.58 Ma and younger), which is clearly aggradational in character and thicker than the Zanclean and Piacenzian wedges, which are instead progradational (Duvail et al., 2005) and therefore suggest a tectonically more stable hinterland than subsequently during the Pleistocene.

Terrace T5 (1.1 Ma) was dated at Villefranche but its most elevated outlier is situated at Fontpédrouse at 1243 m, i.e. half-way between the modern Têt channel (~1000 m at Fontpédrouse) and the present-day altitude of the Late Neogene pediment of La Perche (projecting to ~1500 m at Fontpédrouse; Fig. 4a and b; Fig. 5). An acceleration of uplift since 1.1 Ma, involving a total magnitude of +236 m, can be inferred. It increased after the emplacement of T2 (see section 6.3). On the Roussillon plain, the mean gradient of T5 (calculated between Ille-sur-Têt and Canet) is 0.68%, i.e. slightly less than half the gradient of the stratigraphic boundary between the continental and marine Pliocene units (i.e. 1.24%) and nearly twice the current channel gradient (0.39%). This evidence also indicates an acceleration of tilting since 1.1 Ma as a result of uplift in the hinterland.

6.4.2. Knickzones and faults

Regional uplift of the Axial Zone and its intermontane sedimentary basins also involved localised fault movements. The most spectacular location is revealed by the depth of post-T2 incision above Thuès, and likewise by the thickness of the T2 deposit at that location (Fig. 7a). This unusually straight reach of the river follows the Neogene Têt Fault and is preceded upstream by a series of entrenched meanders through the Mont-Louis bedrock knickzone. The anomaly ends at the Thuès gorge, also featuring a deeply entrenched meander where the river enters the Conflent graben (Figs. 2 and 3). These features suggest a post-T2 reactivation of the tectonic hinge zone that separates the Conflent Basin from the higher massifs. The large thickness of the T2 deposit is more difficult to explain because the T1 deposit, in contrast, is no different here to anywhere else along the Têt valley. Although the hillside morphology does not suggest any indication of a large rockslope failure that might have locally dammed the valley floor at Thuès, a number of large landslides occur farther upstream (Fig. 4e), with the slipped masses resting on the tread of T2. These slope deposits have been nourishing T2 further downstream, as revealed by debris-flow exposures along the N 116 road east of Fontpédrouse. Reverse faulting in the Thuès gorge, or instead extensional slip along the Têt Fault — trapping T2 alluvium in a small N70° graben — thus cannot be ruled out. A rock exposure at the Thuès railway level-crossing provides a clue in support of fault reactivation, revealing two vertical N15° and N8° shear zones at the boundary between the granite and the alluvium, with upturned pebbles along the fault plane as a result of dip-slip fault drag. Extensional motion occurring towards the end of the Middle Pleistocene along the oblique segments of the Têt Fault is compatible with the present-day stress field in this area, which is strike-slip and relates to NE–SW compression and NW–SE extension (Rigo et al., 2015). The stress field also explains the numerous rockslope failures in this area, as likewise the fresh appearance of the triangular faceted spurs and narrowness of tributary gorges descending to the Têt valley (Fig. 4b). The bold morphology of the faceted spurs is thus not just ascribable to the presence of highly resistant, recrystallised Hercynian mylonite, as others have concluded from numerical models (Petit and Mouthereau, 2012), but also a partial manifestation of recent neotectonic activity (Briais et al., 1990) — at least at certain positions along the strike of the fault, such as at Thuès.

Farther downstream, the epigenetic gorge at Villefranche does not reveal any particular disturbances in the terrace profiles or the modern channel gradient. In contrast, the knickpoint and narrow meandering bedrock channel at Rodès are associated with — just downstream of the gorge — a sudden increase in relative relief between T2 and T1 because this area has undergone post-Pliocene tectonic reactivation (Fig. 4c) along the Têt Fault (Calvet, 1996). For example, between Ille-sur-Têt and Millas, a succession of N15° to N50° fault planes exhibiting oblique to near-horizontal striations, have been shown to cut through much of the marine and continental Pliocene sequences. The cumulative vertical throw of these left-lateral strike-slip faults was measured using the basal unconformity of the Pliocene sequence and the marine-to-continental facies boundary, and was found to be 100–150 m. Part of the total offset is probably syn-sedimentary, but most of it post-dates the deposition of the continental clastic beds, which are uniformly tilted 5–6° towards the boundary fault. The base of terrace T5 at Ille-sur-Têt is still vertically offset by ~12 m (Fig. 4c).

In the Roussillon Basin, the asymmetric pattern of terrace treads reveals a continuous drift of the river channel towards the south between generation T5 and generation T2 (Fig. 2). This asymmetry was controlled by a southward tectonic tilt, which is also recorded by the marine to continental boundary within the Pliocene sequence (revealed by a large number of drillcores). The tilt was accommodated by N–S and N45° faults, which have vertically offset the boundary as well as the tread of T5. Near Perpignan, T5 has been lowered by ~20 m to the south of the Têt River compared to its elevation to the north (Figs. 6 and 8). These faults have been detected in the field, where they cut through Pliocene outcrops in the Réart watershed and the hills around Perpignan (Calvet, 1996; Wiazemsky et al., 2015). Their continuation beneath the basin has been documented by borehole surveys (Duvail et al., 2001, 2005). A change in the regional stress regime occurred during the late Pleistocene: today, and since the time of T1, the Têt has returned to a more northerly course, where it follows the Têt Fault as far as Millas, then veers to a N110°E direction corresponding to the continuation of the North-Pyrenean Fault between Millas and Le Soler, before adopting a NE–SW direction until it reaches the sea.

Given that the Pliocene outcrops in this part of the valley are lithologically uniform, only recent tectonics can explain these recent Quaternary changes in the drainage pattern.

7. Conclusion

7.1. Palaeoclimatic inferences from geochronological results

Three terrace levels are well constrained by the TCN and ESR age data: (i) The highest level of the sequence, T5, yielded an ESR age of 1099 ± 179 ka. This alluvial unit thus pre-dates the Early to Middle Pleistocene transition and the established prevalence of 100 ka climatic cycles (Head and Gibbard, 2015). (ii) Terrace level T3c, which holds a median position in the sequence, was correlated with MIS10 on the basis of its ESR age of 374 ± 47 ka. It can be hypothesized on that basis that T3a, T3b, and T3d could be the legacies of MIS 8 to MIS 14, perhaps even MIS 16. (iii) Terrace level T2 was ascribed to MIS 6 on the basis of its ESR age of 174 ± 44 ka.

The other ESR results were too imprecise to be of any value for palaeoclimatic correlation. The TCN age profiles on T2, T3c and T3d were also of limited potential because all of the samples, including those at greatest depth below the surface, yielded TCN concentrations indicative of a nuclide steady state. Such conditions are unsuited to obtaining precise exposure ages. This study also reviewed and reexamined fluvial terrace ages previously published in other Pyrenean valleys. In order to test the sensitivity of profile age-modelling to model parameter settings, we relaxed arbitrary model constraints that had been imposed on TCN concentrations in previous studies. Results showed that in vertical profiles where a nuclide steady state has not yet been reached, results previously considered as age outliers in the Garonne, Segre and Ariège watersheds became realigned and consistent with published ages obtained independently with other dating methods in the regional data set (Fig. 13).

7.2. Uplift magnitudes in the quaternary

Despite the shortfall in age precision, which rules out robust correlations between the ages of the alluvial units and marine isotope stages, the ESR and TCN ages were useful as tools for quantifying rates of valley incision, and thus for providing information about post-orogenic uplift rates in the Pyrenees. Quaternary valley incision is a feature throughout the Pyrenean orogen from its Axial Zone to its outer fold belts. This orogen-wide signal rules out any overbearing contribution to mountain uplift from, for example, the flexural response of the Axial Zone to the load of the offshore Pliocene and Quaternary sedimentary prism in the Gulf of Lion. In the Têt watershed, the data also document an acceleration of valley incision. The rates and associated acceleration are comparable to inferences that have been made elsewhere in the Pyrenees, irrespective of whether the watersheds are controlled by Atlantic or Mediterranean base levels.

The geometry of the terrace sequence, which exhibits a hinge zone in the vicinity of the modern coastline (i.e. normally stratified alluvial stack on the continental shelf passing to a vertical fanning pattern of fluvial terraces onshore and into the mountain range), implies landward uptilting and valley incision driven by post-orogenic regional uplift of the Pyrenean mountain range. Even though incision rates do not strictly equate with crustal uplift rates in all circumstances (Gallen et al., 2015), the measured magnitude of valley incision — a maximum of 450–500 m since the Pliocene below the Plateau de La Perche, and >200 m since the deposition of unit T5 — nonetheless provides a useful approximation of the magnitude of regional uplift (Kiden and Törnqvist, 1998; Maddy, 1998). These approximations are confirmed by stratigraphic markers in the Pliocene sedimentary sequence of the Roussillon Basin, where evidence of westward uptilting of the basin fill sequence, for example, is provided by the gradient of the marine to continental stratigraphic boundary from −200 m near the coastline (Canet borehole data) to +280 m at Vinça. Hypothetically exending this gradient into the Axial Zone to the west would strike the ~770 m elevation contour, suggesting a palaeoelevation of the upper Têt watershed (e.g., the Plateau de la Perche) at the beginning of the Pliocene of merely ~800 m. This regional uptilt motion also involved more localised fault displacement and a sideward tilt of the Roussillon Basin, which controls the planform geometry of terrace outcrops in that area. Evidence of fault motion prior to, during, and after the deposition of unit T2 has been recorded in the field (Calvet, 1996, 1999; Goula et al., 1999), including a change in stress field between the times of T2 and T1 deposition. This is reflected in the response of the Têt River, which underwent northward channel migration in the Roussillon Basin after a long period of southward migration between the times of T5 and T2.

The deformation recorded since the Pliocene and its acceleration during the Quaternary were likely the consequence of conspiring processes: (i) the continuation of dynamic regional uplift caused by shallow asthenosphere inferred to be eroding the base of the lithosphere and causing a strong dynamic response (Pous et al., 1995; Gunnell et al., 2008, 2009; Vanderhaege and Grabkowiak, 2014); and (ii) a minority contribution from flexural uplift in response to denudational unloading of the Axial Zone as a result of glacial and fluvial processes during the Pleistocene (see Suppl. Information 7 for a quantified estimate of the small isostatic component).

Acknowledgements

TCN dating of the alluvial profiles was funded by the Bureau des Recherches Géologiques et Minières through the RGF AMI-Pyr programme. ESR dating was funded by UMR-CNRS 7194 Histoire Naturelle de l'Homme Préhistorique. The ASTER AMS national facility (CEREGE, Aix-en-Provence) is supported by the INSU/CNRS, by the ANR through the 'Projets thématiques d'excellence' programme for the 'Equipements d'excellence' ASTER-CEREGE initiative, and by the Institut de Recherche pour le Développement. The authors thank Gilles Rixhon and an anonymous referee for the constructive remarks on the manuscript.

Appendix A. Supplementary data

Supplementary data related to this article can be found at https://doi.org/10.1016/j.quascirev.2018.06.001.

References

Aguilar, J.P., Michaux, J., 1987. Essai d'estimation du pouvoir séparateur de la méthode biostratigraphique des lignées évolutives chez les rongeurs néogènes. Bulletin Société Géologique de France 8, 1113–1124.

Aguilar, J.P., Lazzari, V., Michaux, J., Sabatier, M., Calvet, M., 2007. Lo Fournas 16-M (Miocène supérieur) et Lo Fournas 16-P (Pliocène moyen), nouvelles localités karstiques à Baixas, Sud de la France): partie I - description et implications géodynamiques. Géologie de la France 1, 55–62.

Agusti, J., Roca, E., 1987. Síntesis bioestratigráfica de la fosa de la Cerdanya (Pirineos orientales). Estud. Geol. (Madr.) 43, 521–529.

Ambert, P., 1994. L'évolution géomorphologique du Languedoc central depuis le Néogène (Grands Causses méridionaux–Piémont languedocien), p. 210. Documents du BRGM 231, Editions BRGM, Orléans.

Antoine, P., Lautridou, J.P., Laurent, M., 2000. Long-term fluvial archives in NW France: response of the Seine and Somme rivers to tectonic movements, climate variations and sea-level changes. Geomorphology 33, 183–207.

Autran, A., Calvet, M., Delmas, M., 2005. Carte géologique de la France (1:50,000 scale), sheet Mont-Louis (1094). Bureau des Recherches Géologiques et Minières, Orléans, p. 107. Explanatory handbook: Laumonier, B., Calvet, M., Delmas, M., Barbey, P., Lenoble, J.-L., Autran, A., 2017.

Bachelet, B., Aguilar, J.P., Calvet, M., Michaux, J., 1990. Nouvelles faunes de rongeurs du Pliocène des Pyrénées orientales: conséquences pour le genre Stephanomys. Geobios 23, 117–120.
Barrère, P., Calvet, M., Courbouleix, S., Gil Peña, I., Martin Alfageme, S., 2009. In: Courbouleix, S., Barnolas, A. (Eds.), Carte géologique du Quaternaire des Pyrénées, vol. 1, 400,000 scale. BRGM and ITGM.
Beaudoin, C., Suc, J.P., Acherki, N., Courtois, L., Rabineau, M., Aloisi, J.C., Javier Sierro, F., Oberlin, C., 2005. Palynology of the northwestern Mediterranean shelf (Gulf of Lions): first vegetational record for the last climatic cycle. Mar. Petrol. Geol. 22, 845–863.
Benito, G., Pérez-González, A., Gutiérrez, F., Machado, M.J., 1998. River response to Quaternary large-scale subsidence due to evaporite solution (Gállego River, Ebro Basin, Spain). Geomorphology 22, 243–263.
Benito, G., Sancho, C., Peña, J.L., Machado, M.J., Rhodes, E.J., 2010. Large-scale karst subsidence and accelerated fluvial aggradation during MIS6 in NE Spain: climatic and paleohydrological implications. Quat. Sci. Rev. 29, 2694–2704.
Berger, G., Clauzon, G., Michaux, J., Suc, J.P., Aloïsi, J.C., Monaco, A., Got, H., Augris, C., Gadel, F., Buscail, R., 1988. Carte géologique de la France (1:50,000 scale), sheet Perpignan (1091). Bureau des Recherches Géologiques et Minières, Orléans, p. 40. Explanatory handbook: Clauzon, G., Berger, G., Aloïsi, J.C., Got, H., Monaco, A., Martin-Buscail, R., Gadel, F, Augris, C., Marchal, J.P., Michaux, J., Suc, J.P., 1989.
Bevington, P., Robinson, K., 2003. Data Reduction and Error Analysis for the Physical Sciences. Mc Graw-Hill Higher Education, p. 336.
Birot, P., 1937. Recherches sur la morphologie des Pyrénées orientales franco-espagnoles. Baillière Editions, p. 318.
Blum, M., Törnqvist, T., 2000. Fluvial responses to climate and sea-level change: a review and look forward. Sedimentology 47, 2–48.
Bosch, G.V., Van Den Driessche, J., Babault, J., Robert, A., Carballo, A., Le Carlier, C., Loget, N., Prognon, C., Wyns, R., Baudin, T., 2016. Peneplanation and lithosphere dynamics in the Pyrenees. Compt. Rendus Geosci. 348, 194–202.
Bourguignon, L., Crochet, J.Y., Capdevila, R., Ivorra, J., Antoine, P.O., Agustí, J., Barsky, D., Blain, H.-A., Boulbes, N., Bruxelles, L., Claude, J., Cochard, D., Filoux, A., Firmat, C., Lozano-Fernandez, I., Magniez, P., Pelletier, M., Rios-Garaizar, J., Testu, A., Valensi, P., De Weyer, L., 2015. Bois-de-Riquet (Lézignan-la-Cèbe, Hérault): a late Early Pleistocene archeological occurrence in southern France. Quat. Int. 393, 24–40.
Bourguignon, L., Barsky, D., Ivorra, J., de Weyer, L., Cuartero, F., Capdevila, R., Cavallina, C., Oms, O., Bruxelles, L., Crochet, J.Y., Rios Garaizar, J., 2016. The stone tools from stratigraphical unit 4 of the Bois-de-Riquet site (Lézignan-la-Cèbe, Hérault, France): a new milestone in the diversity of the European Acheulian. Quat. Int. 411, 160–181.
Braucher, R., Brown, E.T., Bourlès, D.L., Colin, F., 2003. In situ produced ^{10}Be measurements at great depths: implications for production rates by fast muons. Earth Planet Sci. Lett. 211, 251–258.
Braucher, R., Del Castillo, P., Siame, L., Hidy, A., Bourlès, D., 2009. Determination of both exposure time and denudation rate from an in situ-produced ^{10}Be depth profile: a mathematical proof of uniqueness. Model sensitivity and applications to natural cases. Quat. Geochronol. 4, 56–67.
Braucher, R., Merchel, S., Borgomano, J., Bourlès, D.L., 2011. Production of cosmogenic radionuclides at great depth: a multi-element approach. Earth Planet Sci. Lett. 309, 1–9.
Brennan, B.J., 2003. Beta doses to spherical grains. Radiat. Meas. 37, 299–303.
Briais, A., Armijo, R., Winter, T., Tapponnier, P., Herbecq, A., 1990. Morphological evidence for Quaternary normal faulting and seismic hazard in the Eastern Pyrenees. Ann. Tect. 19–42. IV, 1.
Bridgland, D.R., Westaway, R., 2014. Quaternary fluvial archives and landscape evolution: a global synthesis. Proc. Geologists' Assoc. 125, 600–629.
Bridgland, D.R., Demir, T., Seyrek, A., Daoud, M., Abou Romieh, M., Westaway, R., 2017. River terrace development in the NE Mediterranean region (Syria and Turkey): patterns in relation to crustal type. Quat. Sci. Rev. 166, 307–323.
Brocard, G.Y., van der Beek, P.A., Bourlès, D.L., Siame, L.L., Mugnier, J.-L., 2003. Long-term fluvial incision rates and postglacial river relaxation time in the French Western Alps from ^{10}Be dating of alluvial terraces with assessment of inheritance, soil development and wind ablation effects. Earth Planet Sci. Lett. 209, 197–214.
Bull, W.B., 1991. Geomorphic Responses to Climatic Change. Oxford University Press, Oxford, p. 326.
Calle, M., Sancho, C., Peña, J.L., Cunha, P., Oliva-Urcia, B., Pueyo, E., 2013. La secuencia de terrazas cuaternarias del río Alcanadre (provincia de Huesca): caracterización y consideraciones paleoambientales. Cuadernos de Investigación Geográfica 39, 159–178.
Calvet, M., 1986. Les terrasses alluviales de la Têt: étude granulométrique et pétrographique des galets. Rev. Geogr. Pyrenees Sud-Ouest 57, 231–246.
Calvet, M., 1996. Morphogenèse d'une montagne méditerranéenne: les Pyrénées orientales. Documents du BRGM 255 (3), 1177.
Calvet, M., 1999. Régime des contraintes et volumes de relief dans l'Est des Pyrénées. Géomorphologie: relief, processus. Environnement 3, 253–278.
Calvet, M., Serrat, P., Lemartinel, B., Marichal, R., 2002. Les cours d'eau des Pyrénées orientales depuis 15000 ans. Etat des connaissances et perspectives de recherche. In: Bravard, J.P., Magny, M. (Eds.), (Dir.) Histoire des rivières et des lacs du Lascaux à nos jours. Errances, Paris, pp. 279–294.
Calvet, M., Gunnell, Y., 2008. Planar landforms as markers of denudation chronology: an inversion of East Pyrenean tectonics based on landscape and sedimentary basin analysis. In: Gallagher, K., Jones, S.J., Wainwright, J. (Eds.), Landscape Evolution: Denudation, Climate and Tectonics over Different Time and Space Scales, vol. 296. Geological Society of London, Special Publication, pp. 147–166.
Calvet, M., Delmas, M., Gunnell, Y., Braucher, R., Bourlès, D., 2011. Recent advances in research on Quaternary glaciations in the Pyrenees. In: Ehlers, J., Gibbard, P.L., Hughes, P. (Eds.), Quaternary Glaciations, Extent and Chronology, a Closer Look Part IV. Elsevier, Amsterdam, pp. 127–139.
Calvet, M., Gunnell, Y., Braucher, R., Hez, G., Bourles, D., Guillou, V., Delmas, M., Aster Team, 2015a. Cave levels as proxies for measuring post-orogenic uplift: evidence from cosmogenic dating of alluvium-filled-cave in the French Pyrenees. Geomorphology 246, 617–633.
Calvet, M., Autran, A., Wiazemsky, M., Laumonier, B., Guitard, G., 2015b. Carte géologique de la France (1:50,000 scale), sheet Argelès-sur-Mer–Cerbère (1097). Bureau des Recherches Géologiques et Minières, Orléans, p. 149. Explanatory handbook: Laumonier B., Calvet M., Barbey P., Guennoc P., Lambert J., Lenoble J.-L., Wiazemsky M., 2015.
Carcaillet, J., Mugnier, J.L., Koçi, R., Jouanne, F., 2009. Uplift and active tectonics of southern Albania inferred from incision of alluvial terraces. Quat. Res. 71, 465–476.
Carozza, J.M., Delcaillau, B., 1999. L'enregistrement géomorphologique de la tectonique quaternaire par les nappes alluviales: l'exemple du bassin de la Têt (Roussillon, France). Compte Rendu Académie des Sciences, Paris. Sciences de la Terre Planètes 329, 735–740.
Carozza, J.M., Puig, C., 2011. Changements environnementaux, vulnérabilité et adaptation des sociétés du passé: l'exemple du Petit âge glaciaire en Roussillon. Sud-Ouest Eur. 32, 67–79.
Carozza, J.M., Puig, C., Odiot, T., Valette, P., Passarius, O., 2011. Lower mediterranean plain accelerated evolution during the little ice age: geoarcheological insight in the Tech basin (Roussillon, Gulf of lion, western mediterranean). Quat. Int. 266, 94–104.
Carozza, J.M., Puig, C., Odiot, T., Passarius, O., Valette, P., 2013. L'édification de la Basse Plaine de la Salanque (Roussillon, France) au cours de la seconde partie de l'holocène et ses implications sur la répartition des sites archéologiques. Quaternaire 24, 155–165.
Carozza, J.M., Llubes, M., Danu, M., Faure, E., Carozza, L., David, M., Manen, C., 2016. Geomorphological evolution of mediterranean enclosed depressions in the late glacial and Holocene: the example of canohès (Roussillon, SE France). Geomorphology 273, 78–92.
Clauzon, G., 1990. Restitution de l'évolution géodynamique néogène du bassin du Roussillon et de l'unité adjacente des Corbières d'après les données écostratigraphiques et paléogéographiques. Paleobiol. Cont. 17, 125–155.
Clauzon, G., Aguilar, J.P., Michaux, J., 1987. Le bassin pliocène du Roussillon (Pyrénées-Orientales, France): exemple d'évolution géodynamique d'une ria méditerranéenne consécutive à la crise de salinité messinienne. Compte Rendus de l'Académie des Sciences, Paris, série II 304, 585–590.
Clauzon, G., Cravatte, J., 1985. Révision chronostratigraphique de la série marine pliocène traversée par le sondage Canet 1 (Pyrénées-Orientales) : apport à la connaissance du Néogène du Roussillon. Compte Rendus de l'Académie des Sciences, Paris, série II 301, 1351–1354.
Clauzon, G., Suc, J.P., Aguilar, J.P., Ambert, P., Capetta, H., Cravatte, J., Drivaliari, A., Domenech, R., Dubar, M., Leroy, S., Martinell, J., Michaux, J., Roiron, P., Rubino, J.L., Savoye, B., Vernet, J.L., 1990. Pliocene geodynamic and climatic evolutions in the French mediterranean region. In: Agustí, J., Domènech, R., Julià, R., Martinell, J. (Eds.), Berian Neogene Basins, Field Guidebook. Paleontologia I Evolució, Memoria Especial n° 2, pp. 131–186.
Collina-Girard, J., 1975. Les industries archaïques sur galets des terrasses quaternaires de la plaine du Roussillon. MPhil. Dissertation. Univ. Provence, p. 408.
Collina-Girard, J., 1976. Les alluvions fluviatiles des fleuves côtiers dans le Roussillon. In: de Lumley, H. (Ed.), La Préhistoire Française. CNRS édit, pp. 78–82.
Cordier, S., Adamson, K., Delmas, M., Calvet, M., Harmand, D., 2017. Of ice and water: quaternary fluvial response to climate forcing in glacially influenced river systems. Quat. Sci. Rev. 166, 57–73.
Counts, R.,C., Murari, M.K., Owen, L.A., Mahan, S.A., Greenan, M., 2015. Late Quaternary chronostratigraphic framework of terraces and alluvium along the lower Ohio River, southwestern Indiana and western Kentucky, USA. Quat. Sci. Rev. 110, 72–91.
Debals, B., 1998. PhD thesis (unpubl.). Étude sédimentologique des formations quaternaires des bassins des fleuves côtiers du Roussillon (France): vallées de la Têt et du Tech, vol. 2. Univ. Perpignan, p. 288.
Debals, B., 2000. Mise au point sur la chronostratigraphie des dépôts alluviaux quaternaires de la plaine du Roussillon: exemple de la vallée de la Têt (France). Quaternaire 11, 31–39.
Delmas, M., Calvet, M., Gunnell, Y., 2009. Variability of erosion rates in the Eastern Pyrenees during the last glacial cycle—a global perspective with special reference to the Eastern Pyrenees. Quat. Sci. Rev. 28, 484–498.
Delmas, M., Calvet, M., Gunnell, M., Braucher, R., Bourlès, D., 2011. Palaeogeography and ^{10}Be exposure-age chronology of Middle and Late Pleistocene glacier systems in the northern Pyrenees: implications for reconstructing regional palaeoclimates. Palaeogeogr. Palaeoclimatol. Palaeoecol. 305, 109–122.
Delmas, M., Braucher, R., Gunnell, Y., Guillou, V., Calvet, M., Bourlès, D., 2015. Constraints on Pleistocene glaciofluvial terrace age and related soil chronosequence features from vertical ^{10}Be profiles in the Ariège River catchment (Pyrenees, France). Global Planet. Change 132, 39–53.
Demoulin, A., Mather, A., Whittaker, A., 2017. Fluvial archives, a valuable record of vertical crustal deformation. Quat. Sci. Rev. 166, 10–37.
Dubar, M., 1986. Cartographie des formations superficielles dans les Corbières

méridionales (sheet Tuchan, 1:50,000 scale). Rev. Geogr. Pyrenees Sud-Ouest 57, 247–256.
Dubreuilh, J., Capdeville, J.-P., Farjanel, G., Karnay, G., Platel, J.-P., Simon-Coincon, R., 1995. Dynamique d'un comblement continental néogène et quaternaire: l'exemple du bassin d'Aquitaine. Geologie de la France 4, 3–26.
Durand, B., Jolivet, L., Horvath, F., Séranne, M. (Eds.), 1999. The Mediterranean Basins: Tertiary Extension within the Alpine Orogen, vol. 156. Geological Society of London, Special Publication, p. 570.
Duvail, C., 2008. PhD thesis (unpubl.). Expression des facteurs régionaux et locaux dans l'enregistrement sédimentaire d'une marge passive. Exemple de la marge du Golfe du Lion étudiée selon un continuum terre-mer, vol. 2. Univ. Montpellier, p. 295.
Duvail, C., Le Strat, P., 2000. Evolution géodynamique du bassin du Roussillon: Analyse des profils sismiques calibrés par des sondages profonds de Elne1 et de Canet1. GEO-TERRE Report, p. 23. GTR/BRGM/12000–12137.
Duvail, C., Le Strat, P., Bourgine, B., 2001. Atlas géologique des formations plio-quaternaires de la plaine du Roussillon (Pyrénées Orientales). BRGM Report, BRGM/RP-51197-FR, p. 44.
Duvail, C., Le Strat, P., , avec la collaboration, de Gorini, C., Lofi, J., Clauzon, G., 2002. Architecture et géométrie haute résolution des prismes sédimentaires plio-quaternaires au droit du Roussillon suivant un profil terre-mer. BRGM report BRGM/RP-51972-FR, p. 71.
Duvail, C., Gorini, C., Lofi, J., Le Strat, P., Clauzon, G., Dos Reis, T., 2005. Correlation between onshore and offshore pliocene–quaternary systems tracks below the Roussillon Basin (eastern Pyrenees, France). Mar. Petrol. Geol. 22, 747–756.
Finnegan, N.J., Schumer, R., Finnegan, S., 2014. A signature of transience in bedrock river incision rates over timescales of 104–107 years. Nature 505, 391–394.
Fonteilles, M., Leblanc, D., Clauzon, G., Vaudin, J.L., Berger, G.M., 1993. Carte géologique de la France (1:50,000 scale), sheet Rivesaltes (1090). Bureau des Recherches Géologiques et Minières, Orléans, p. 119. Explanatory handbook: Berger, G.M., Fonteilles, M., Leblanc, D., Clauzon, G., Marchal, J.P., Vautrelle, C., 1993.
Fuchs, M.C., Gloagen, R., Pohl, E., 2013. Tectonic and climatic forcing on the Panj river system during the Quaternary. Int. J. Earth Sci. 102, 1985–2003.
Fuchs, M.C., Gloaguen, R., Krbetschekb, M., Szulc, A., 2014. Rates of river incision across the main tectonic units of the Pamir identified using optically stimulated luminescence dating of fluvial terraces. Geomorphology 216, 79–92.
Gallen, S.F., Pazzaglia, F.J., Wegmann, K.W., Pederson, J.L., Gardner, T.W., 2015. The dynamic reference frame of rivers and apparent transience in incision rates. Geology 43, 623–626.
Gao, H., Li, Z., Liu, X., Pan, B., Wu, Y., Liu, F., 2017. Fluvial terraces and their implications for Weihe River valley evolution in the Sanyangchuan Basin. SCIENCE China. Earth Sci. 60, 413–427.
García-Ruiz, J.M., Martí-Bono, C., Peña-Monné, J.L., Sancho, C., Rhodes, E., Valero, B., Gonzalez Samperiz, P., Moreno, A., 2013. Glacial and fluvial deposits in the Aragón Valley, central western Pyrenees: chronology of the Pyrenean late Pleistocene glaciers. Geogr. Ann.: Series A Physical Geography 95, 15–32.
Gibbard, P.L., Lewin, J., 2009. River incision and terrace formation in the late Cenozoic of Europe. Tectonophysics 474, 41–55.
Giresse, P., Martzluff, M., 2015. AMS radiocarbon dating of carbonate cements in late Pleistocene alluvial conglomerates, Verdouble River. Palaeoenvironmental implications concerning the Palaeolithic site of Tautavel (Pyrénées-Orientales). Géomorphol. Relief, Process. Environ. 21, 115–130.
Giret, A., 1995. Etude des déformations quaternaires de la Têt par l'analyse morphométrique. Bull. Assoc. Fr. Étude Quat. 6, 121–137.
Giret, A., 2014. Le Quaternaire fluvial et torrentiel du Roussillon. Présence graphique-Monts, Tours, p. 162.
Gorini, C., Lofi, J., Duvail, C., Dos Reis, T., Guennoc, P., Le Strat, P., Mauffret, A., 2005. The Late Messinian salinity crisis and Late Miocene tectonism: interaction and consequences on the physiography and post-rift evolution of the Gulf of Lions margin. Mar. Petrol. Geol. 22, 695–712.
Goula, X., Olivera, C., Fleta, J., Grellet, B., Lindo, R., Rivera, L.A., Cisternas, A., Carbon, D., 1999. Present and recent stress regime in the eastern part of the Pyrenees. Tectonophysics 308, 487–502.
Guitard, G., Geyssant, J., Laumonier, M., Autran, A., Fonteilles, M., Dalmayrach, B., Vidal, J.C., Bandet, Y., 1992. Carte géologique de la France (1:50,000 scale), sheet Prades (1095). Bureau des Recherches Géologiques et Minières, Orléans, p. 198. Explanatory handbook: Guitard, G., Laumonier B., Autran, A., Bandet, Y., Berger, G.M., 1998.
Gunnell, Y., Zeyen, H., Calvet, M., 2008. Geophysical evidence of a missing lithospheric root beneath the eastern Pyrenees: consequences for post-orogenic uplift and associated geomorphic signatures. Earth Planet Sci. Lett. 276, 302–313.
Gunnell, Y., Calvet, M., Brichau, S., Carter, A., Aguilar, J.P., Zeyen, H., 2009. Low long-term erosion rates in high-energy mountain belts: insights from thermo- and biochronology in the eastern Pyrenees. Earth Planet Sci. Lett. 278, 208–218.
Hancock, G.S., Anderson, R.S., Chadwick, O.A., Finkel, R.C., 1999. Dating fluvial terraces with ^{10}Be and ^{26}Al profiles: application to the Wind River, Wyoming. Geomorphology 27, 41–60.
Head, M., Gibbard, P.L., 2015. Early–Middle Pleistocene transitions: linking terrestrial and marine realms. Quat. Int. 389, 7–46.
Hernandez, M., Mercier, N., Bertran, P., Colonge, D., Lelouvier, L.A., 2012. Premiers éléments de datation des industries du Pléistocène moyen (Acheuléen–Paléolithique moyen ancien) de la région pyrénéo-garonnaise: une approche géochronologique pluri-méthodes (TL, OSL et TT-OSL) des sites de Duclos et Romentères. Paléo 23, 155–170.
Hidy, A.J., Gosse, J.C., Pederson, J.L., Mattern, J.P., Finkel, R.C., 2010. A geologically constrained Monte Carlo approach to modeling exposure ages from profiles of cosmogenic nuclides: an example from Lees Ferry, Arizona. G-cubed 11. https://doi.org/10.1029/2010GC003084. Q0AA10.
Hubschman, J., 1975a. Les terrasses récentes de la Garonne et leur évolution. Bull. Assoc. Fr. Étude Quat. 12, 137–147.
Hubschman, J., 1975b. L'évolution des nappes alluviales antérissiennes de la Garonne dans l'avant-pays molassique. Bull. Assoc. Fr. Étude Quat. 12, 149–169.
Hubschman, J., 1975c. Morphogenèse et pédogenèse quaternaire dans le piémont des Pyrénées garonnaises et ariégeoises. Thèse de Doctorat d'Etat. Université de Toulouse-le-Mirail, p. 745 (1974).
Hubschman, J., 1975d. Le plateau de Lannemezan. Bull. Assoc. Fr. Étude Quat. 12, 207–209.
Icole, M., 1974. Géochimie des altérations dans les nappes d'alluvions du piémont Occidental nord-pyrénéen. Eléments de paléopédologie quaternaire. Sci. Geol. 40, 200. Université Louis Pasteur, Strasbourg.
Kiden, P., Törnqvist, T.E., 1998. Can river terrace flights be used to quantify Quaternary tectonic uplift rates? J. Quat. Sci. 13, 573–574.
Lacan, P., Ortuño, M., 2012. Active tectonics of the Pyrenees: a review. J. Iber. Geol. 38, 9–30.
Labaune, C., Tesson, M., Gensous, B., 2005. Integration of high and very high-resolution seismic reflection profiles to study Upper Quaternary deposits of a coastal area in the western Gulf of Lions, SW France. Mar. Geophys. Res. 26, 109–122.
Labeyrie, J., Lalou, C., Monaco, A., Thommeret, J., 1976. Chronologie des niveaux eustatiques sur la côte du Roussillon de -33 000 ans à nos jours. Compte Rendu de l'Académie des Sciences de Paris série D 282, 349–352.
Lehner, B., Grill, G., 2013. Global river hydrography and network routing: baseline data and new approaches to study the world's large river systems. Hydrol. Process. 27, 2171–2186.
Leopold, L.B., Wolman, L.G., Miller, J., 1964. Fluvial Processes in Geomorphology. W.H. Freeman, San Francisco, p. 522.
Lewis, C.J., McDonald, E.V., Sancho, C., Peña, J.L., Rhodes, E.J., 2009. Climatic implications of correlated Upper Pleistocene and fluvial deposits on the Cinca and Gállego Rivers (NE Spain) based on OSL dating and soil stratigraphy. Global Planet. Change 67, 141–152.
Lewis, C.J., Sancho, C., McDonald, E.V., Peña-Monné, J.L., Pueyo, E.L., Rhodes, E., Calle, M., Soto, R., 2017. Post-tectonic landscape evolution in NE Iberia using staircase terraces: combined effects of uplift and climate. Geomorphology 292, 85–103.
Lisiecki, L.E., Raymo, M.E., 2005. A Pliocene-Pleistocene stack of 57 globally distributed benthic d^{18}O records. Paleoceanography 20, PA1003. https://doi.org/10.1029/2004PA001071.
Lobo, J.F., Tesson, M., Gensous, B., 2004. Stratral architectures of late quaternary regressive–transgressive cycles in the Roussillon shelf (SW Gulf of lions, France). Mar. Petrol. Geol. 21, 1181–1203.
Ludwig, K.R., 2003. User's Manual for Isoplot/Ex, Version 3.0, a Geochronological Toolkit for Microsoft Excel. Special Publication, v. 4. Berkeley Geochronology Center, p. 75.
Maddy, D., 1997. Uplift-driven valley incision and river terrace formation in southern England. J. Quat. Sci. 12, 539–545.
Maddy, D., 1998. Reply: can river terrace flights be used to quantify Quaternary tectonic uplift rates? J. Quat. Sci. 13, 574–575.
Maddy, D., Bridgland, D.R., 2000. Accelerated uplift resulting from Anglian glacioisostaticrebound in the Middle Thames Valley, UK: evidence from the river terrace record. Quat. Sci. Rev. 19, 1581–1588.
Maddy, D., Bridgland, D.R., Green, C.P., 2000. Crustal uplift in southern England: evidence from the river terrace record. Geomorphology 33, 167–181.
Merritts, D.J., Vincent, K.R., Wohl, E.E., 1994. Long river profiles, tectonism, and eustacy: a guide to interpreting fluvial terraces. J. Geophys. Res. 99, 14031–14050.
Monaco, A., 1973. The Roussillon continental margin (Gulf of Lions): plio-quaternary paleogeographic interpretation. Sediment. Geol. 10, 261–284.
Monaco, A., Thommeret, J., Thommeret, Y., 1972. L'âge des dépôts quaternaires sur le plateau continental du Roussillon (golfe du Lion). Compte Rendus de l'Académie des Sciences, Paris, Série D 274, 2280–2283.
Moreno, D., Falguères, C., Perez-Gonzalez, C., Duval, M., Voinchet, P., Benito-Calvo, A., Ortega, A.I., Bahain, J.J., Sala, R., Carbonell, E., Bermúdez de Castro, J.M., Arsuaga, J.L., 2012. ESR chronology of alluvial deposits in the Arlanzon valley (Atapuerca, Spain): contemporaneity with Atapuerca Gran Dolina site. Quat. Geochronol. 10, 418–423.
Mouchené, M., van der Beek, P., Mouthereau, F., Carcaillet, J., 2017. Controls on quaternary incision of the northern pyrenean foreland: chronological and geomorphological constraints from the lannemezan megafan, SW France. Geomorphology 281, 78–93.
Nivière, B., Lacan, P., Regard, V., Delmas, M., Calvet, M., Huyghe, D., Roddaz, B., 2016. Evolution of the late Pleistocene Aspe river (western Pyrenees, France). Signature of climatic events and active tectonics. Compt. Rendus Geosci. 348, 203–212.
Olszak, J., 2017. Climatically controlled terrace staircases in uplifting mountainous areas. Global Planet. Change 153, 13–23.
Ortuño, M., Queralt, P., Martí, A., Ledo, J., Masana, E., Perea, H., Santanach, P., 2008. The North Maladeta Fault (Spanish Central Pyrenees) as the Vielha 1923 earthquake seismic source: recent activity revealed by geomorphological and

geophysical research. Tectonophysics 453, 246–262.
Ortuño, M., Marti, A., Martin-Closas, C., Jimenez-Moreno, G., Martinetto, E., Santanach, P., 2013. Paleoenvironments of the Late Miocene Prüedo Basin: Implications for the Uplift of the Central Pyrenees. Journal of the Geological Society, London 170, 79–92.
Pan, B., Burbank, D., Wang, Y., Wu, G., Li, J., Guan, Q., 2003. A 900 k.y. record of strath terrace formation during glacial-interglacial transitions in northwest China. Geology 31, 957–960.
Pan, B., Su, H., Hua, Z., Hu, X., Gao, H., Li, J., Kirby, E., 2009. Evaluating the role of climate and tectonics during non-steady incision of the Yellow River: evidence from a 1.24 Ma terrace record near Lanzhou, China. Quat. Sci. Rev. 28, 3281–3290.
Pazzaglia, F.J., 2013. Fluvial terraces. In: Shroder, J., Wohl, E. (Eds.), Treatise on Geomorphology, vol. 9. Academic Press, San Diego, CA, pp. 379–412. Fluvial Geomorphology.
Peña Monné, J.L., Turu, V., Calvet, M., 2011. Les terrasses fluvials del Segre i afluents principals: descripció d'afloraments i assaig de correlació. In: Turu, V., Constante, A. (Eds.), El Cuaternario en España y áreas afines, avances en 2011, XIII Reunión Nacional de Cuaternario, Andorra, 4-7 juillet, Asociación Española para el Estudio del Cuaternario (AEQUA), pp. 51–55.
Petit, C., Mouthereau, F., 2012. Steep topographic slope preservation by anisotropic diffusion: an example from the Neogene Têt fault scarp, eastern Pyrenees. Geomorphology 171–172, 173–179.
Phillip, H., Bousquet, J.-C., Escuer, J., Fleta, J., Goula, X., Grellet, B., 1992. Présence de failles inverses d'âge quaternaire dans l'Est des Pyrénées: implications sismotectoniques. Compte Rendu Académie des Sciences, Paris, II 314, 1239–1245.
Pous, J., Muñoz, J.A., Ledo, J.J., Liesa, M., 1995. Partial Melting of Subducted continental Lower Crust in the Pyrenees. Journal of the Geological Society, London 152, 217–220.
Rabineau, M., Berné, S., Ledrezen, E., Lericolais, G., Marsset, T., Rotunno, M., 1998. 3D architecture of lowstand and transgressive Quaternary sand bodies on the outer shelf of the Gulf of Lion, France. Mar. Petrol. Geol. 15, 439–452.
Rabineau, M., Berné, S., Aslanian, D., Olivet, J.-L., Joseph, P., Guillocheau, F., Bourrillet, J.-F., Ledrezen, E., Grangeon, D., 2005. Sedimentary sequences in the Gulf of Lion: a record of 100,000 year climatic cycles. Mar. Petrol. Geol. 22, 775–804.
Rabineau, M., Berné, S., Olivet, J.L., Aslanian, D., Guillocheau, F., Joseph, P., 2006. Paleo-sea levels reconsidered from direct observation of paleoshoreline position during Glacial Maxima (for the last 500,000 yr). Earth Planet Sci. Lett. 252, 119–137.
Rabineau, M., Leroux, E., Aslanian, D., Bache, F., Gorini, C., Moulin, M., Molliex, S., Droza, L., dosReis, A.T., Rubino, J.L., Guillocheau, F., Olivet, J.L., 2014. Quantifying subsidence and isostatic readjustment using sedimentary paleomarkers, example from the Gulf of Lion. Earth Planet Sci. Lett. 388, 353–366.
Rigo, A., Vernant, P., Feigl, K.L., Goula, X., Khazaradze, G., Talaya, J., Morel, L., Nicolas, J., Baize, S., Chery, J., Sylvander, M., 2015. Present-day deformation of the Pyrenees revealed by GPS surveying and earthquake focal mechanisms until 2011. Geophys. J. Int. 201, 947–964.
Rixhon, G., Briant, B., Cordier, S., Duval, M., Jones, A., Scholz, D., 2017. Revealing the pace of river landscape evolution during the Quaternary: recent developments in numerical dating methods. Quat. Sci. Rev. 166, 91–113.
Ruszkiczay-Rüdiger, Z., Braucher, R., Novothny, A., Csillag, G., Fodor, L., Molnár, G., Madarász, B., ASTER Team, 2016. Tectonic and climatic control on terrace formation: coupling in situ produced ^{10}Be depth profiles and luminescence approach, Danube River, Hungary, Central Europe. Quat. Sci. Rev. 131, 127–147.
Sancho, C., Calle, M., Peña-Monne, J.L., Duval, M., Oliva-Urcia, B., Pueyo, E.L., Benito, G., Moreno, A., 2016. Dating the earliest Pleistocene alluvial terrace of the Alcanadre River (Ebro Basin, NE Spain): insights into the landscape evolution and involved processes. Quat. Int. 407, 86–95.
Sartégou, A., Bourlès, D., Blard, P.H., Braucher, R., Tibaric, B., Zimmermann, L., Leanni, L., ASTER Team, Aumaître, G., Keddadouched, K., 2018. Deciphering landscape evolution with karstic networks: a Pyrenean case study. Quat. Geochronol. 43, 12–29.
Schumm, S.A., 1969. River Metamorphosis. Journal of the Hydraulics Division, vol. 95. American Society of Civil Engineers, pp. 255–273.
Schumm, S.A., 1973. Geomorphic thresholds and complex responses of drainage systems. In: Morisawa, M. (Ed.), Fluvial Geomorphology. Binghamton Publications in Geomorphology, vol. 3, pp. 299–310.
Schumm, S.A., 1977. The Fluvial System. Wiley, New York, p. 338.
Schumm, S.A., 1979. Geomorphic thresholds: the concept and its applications. Transactions of the Institute of British geographers. New Series 4, 485–515.
Schumm, S.A., 2007. River Variability and Complexity. Cambridge University Press, Cambridge, p. 220.
Schumm, S.A., Parker, R.S., 1973. Implications of complex response of drainage systems for quaternary alluvial stratigraphy. Nature 243, 99–100.
Silva, P.G., Roquero, E., Lopez-Recio, M., Huerta, P., Martínez-Graña, A.M., 2017. Chronology of fluvial terrace sequences for large Atlantic rivers in the Iberian Peninsula (Upper Tagus and Duero drainage basins, Central Spain). Quat. Sci. Rev. 166, 188–203.
Stange, K.M., Van Balen, R., Vandenberghe, J., Peña, J.L., Sancho, C., 2012. External controls on quaternary fluvial incision and terrace formation at the Segre River, southern Pyrenees. Tectonophysics 602, 316–331.
Stange, K.M., Van Balen, R.T., Carcaillet, J., Vandenberghe, J., 2013. Terrace staircase development in the southern Pyrenees foreland: inferences from 10Be terrace exposure ages at the Segre River. Global Planet. Change 101, 97–112.
Stange, K.M., Van Balen, R.T., Kasse, C., Vandenberghe, J., Carcaillet, J., 2014. Linking morphology across the glaciofluvial interface: a 10Be supported chronology of glacier advances and terrace formation in the Garonne River, northern Pyrenees, France. Geomorphology 207, 71–95.
Stange, K.M., Van Balen, T., Garcia-Castellanos, G, R.T., Cloetingh, S., 2016. Numerical modelling of Quaternary terrace staircase formation in the Ebro foreland basin, southern Pyrenees, NE Iberia. Basin Res. 28, 124–146.
Starkel, L., 2003. Climatically controlled terraces in uplifting mountain areas. Quat. Sci. Rev. 22, 2189–2198.
Turu, V., Calvet, M., Bordonau, J., Gunnell, Y., Delmas, M., Vilaplana, J.M., Jalut, G., 2016. Did Pyrenean glaciers dance to the beat of global climatic events? Evidence from the Würmian sequence stratigraphy of an ice-dammed palaeolake depocentre in Andorra. In: Hughes, P.D., Woodward, J.C. (Eds.), Quaternary Glaciation in the Mediterranean Mountains, vol. 433. Geological Society of London. Special Publication. http://doi.org/10.1144/SP433.6.
Vanderhaege, O., Grabkowiak, A., 2014. Tectonic accretion and recycling of the continental lithosphere during the Alpine orogeny along the Pyrenees. Bull. Soc. Geol. Fr. 185, 143–155.
Vincent, K., Chadwick, O.A., 1994. Synthesizing bulk density for soils with abundant rock fragments. Soil Sci. Soc. Am. J. 58, 455–464.
Viveen, W., Braucher, R., Bourlès, D., Schoorl, J.M., Veldkamp, A., Van Balen, R.T., Wallinga, J., Fernandez-Mosquera, D., Vidal-Romani, J.R., Sanjurjo-Sanchez, J., 2012. 0.65 Ma chronology and incision rate assessment of the NW Iberian Miño River terraces based on ^{10}Be and luminescence dating. Global Planet. Change 94–95, 82–100.
Voinchet, P., Toyoda, S., Falguères, C., Hernandez, M., Tissoux, H., Moreno, D., Bahain, J.-J., 2015. Evaluation of ESR residual dose in quartz modern samples, an investigation on environmental dependence. Quat. Geochronol. 30, 506–512.
Wang, X., Vandenberghe, J., Shuangwen, Y., Van Balen, R., Lua, H., 2015. Climate-dependent fluvial architecture and processes on a suborbital timescale in areas of rapid tectonic uplift: an example from the NE Tibetan Plateau. Global Planet. Change 133, 318–329.
Westaway, R., Bridgland, D., White, M., 2006. The Quaternary uplift history of central southern England: evidence from the terraces of the Solent River system and nearby raised beaches. Quat. Sci. Rev. 25, 2212–2250.
Westaway, R., Bridgland, D.R., Sinha, R., Demir, T., 2009. Fluvial sequences as evidence for landscape and climatic evolution in the Late Cenozoic: a synthesis of data from IGCP 518. Global Planet. Change 68, 237–253.
Whipple, K.X., 2004. Bedrock rivers and the geomorphology of active orogens. Annu. Rev. Earth Planet Sci. 32, 151–185.
Whipple, K.X., DiBiase, R.A., Crosby, B.T., 2013. Bedrock rivers. In: Shroder, J., Wohl, E. (Eds.), Treatise on Geomorphology, vol. 9. Academic Press, San Diego, CA, pp. 550–573. Fluvial Geomorphology.
Wiazemsky, M., Calvet, M., Laumonier, B., Guitard, G., Autran, A., Llac, F., Baudin, T., 2010. Carte géologique de la France (1:50,000 scale), sheet Ceret (1096). Bureau des Recherches Géologiques et Minières, Orléans, p. 164. Explanatory handbook: Laumonier, B., Calvet, M., Wiazemsky, M., Barbey, P., Marignac, C., Lambert, J., Lenoble, J.-L., 2015.
Wobus, C., Whipple, K.X., Kirby, E., Snyder, N., Johnson, J., Spyropolou, K., Crosby, B., Sheehan, D., 2006. Tectonics from topography: procedures, promise, and pitfalls. In: Willett, S.D., Hovius, N., Brandon, M.T., Fisher, D. (Eds.), Tectonics, Climate, and Landscape Evolution. Geological Society of America Special Paper, vol. 398, pp. 55–74.
Yokoyama, Y., Falguères, C., Quaegebeur, J.P., 1985. ESR dating of quartz from Quaternary sediments: first attempts. Nucl. Tracks 10, 921–928.